UiT
THE ARCTIC
UNIVERSITY
OF NORWAY

Department of Physics and Technology

Statistical properties of intermittent fluctuations in the boundary of fusion plasmas

—

Audun Theodorsen

A dissertation for the degree of Philosophiae Doctor – June 2018

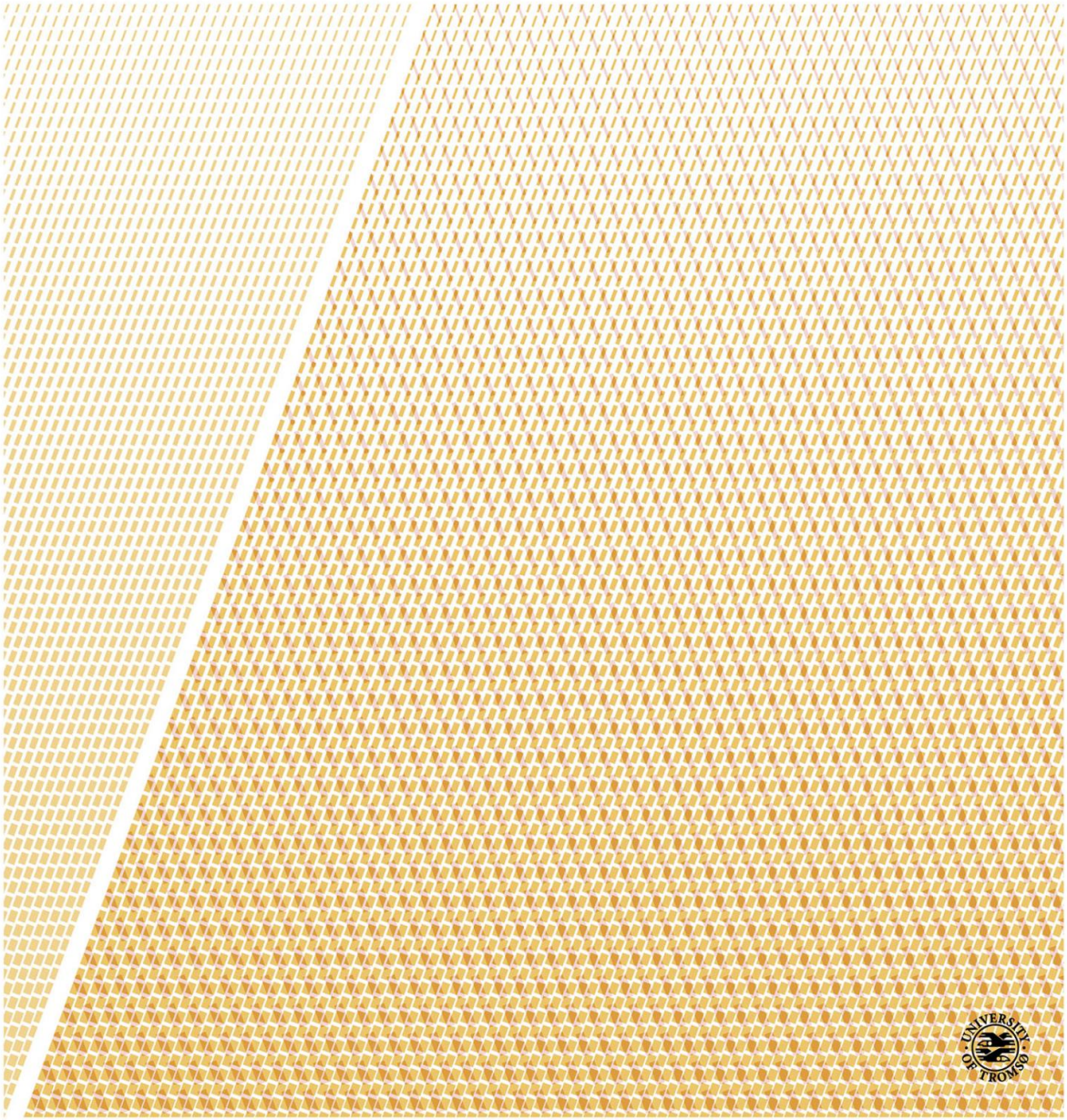

Abstract

Fluctuation-induced plasma–wall interactions is a major concern for the next generation, high duty-cycle magnetic confinement fusion devices. The turbulence is generated in the outboard midplane transition region between the confined core plasma and the scrape-off layer where magnetic field lines intersect material walls. Here, filaments of hot and dense plasma, elongated in the field direction, detach from the main plasma and move radially outwards, driven by interchange motion. These filaments cause enhanced plasma–wall interactions compared to the level estimated by only considering time-averaged plasma parameters, reduce the efficiency of radio frequency wave heating and is likely related to the empirical discharge density limit.

When measured as a time series from a stationary point (either as ion saturation current from electrical probes probes or as emitted light intensity from gas puff imaging), the statistical properties of the turbulent fluctuations in the scrape-off layer are robust across devices, confinement modes and plasma parameters. The highly intermittent fluctuations exhibit skewed and flattened probability density functions and power spectra that are flat for low frequencies and have a power-law tail for high frequencies. Conditional averaging reveals that large-amplitude structures have a sharp, exponential rise and a slower, exponential decay. Both the peak amplitudes of these structures and the waiting time between them are exponentially distributed.

In this thesis, a stochastic model describing the time series as a superposition of uncorrelated, two-sided exponential pulses with exponentially distributed amplitudes arriving according to a Poisson process is analysed and its assumptions and predictions are compared with measurement data. This model is consistent with all the above statistical properties. The predictive capabilities of the model are improved by deriving expressions for the rate of threshold crossings and the time the signal spends above a given threshold level. The effects of additive noise and different amplitude distributions are also considered. Parameter estimation from moments, probability density functions and characteristic functions is examined using Monte-Carlo simulations. The model predictions are favorably compared to measurement data from experiments on the TCV and Alcator C-Mod devices.

Acknowledgements

First, I would like to thank my supervisor, Odd Erik Garcia, for his guidance. Odd Erik has always found the time for short questions and long discussions, and has proofread my work with frightening attention to detail. Any remaining mistakes are my own. I would also like to thank my co-supervisor Martin Rypdal for his contributions and for helping us physicists do our math correctly.

I am grateful to Drs. Brian LaBombard and Jim Terry for hosting me at MIT, for their hospitality and for their insight. I learned much during my time in Boston. Ralph Kube deserves thanks for our discussions and his support, during our travels and academically.

I would like to thank the Department of Physics and Technology, the Faculty of Science and Technology, UiT Campus Harstad and the Plasma Science and Fusion Center at MIT for their administrative support. PSFC also deserves thanks for their generous hospitality. I am grateful to the Reaserch Council of Norway for funding my PhD, my stay at PSFC and my conference travels.

My thanks go to my office mates in Tromsø and the doctoral students in Harstad for our conversations, academic and otherwise. I would also like to thank FKFD Tromsø and Athena School of Arms in Boston, as hitting things with swords solves most problems.

Lastly, I would like to thank Martine for keeping my motivation up and making sure I relax every now and then, and my parents for their support and for helping me navigate academia. Bestemor og bestefar, takk for støtte og middager.

Contents

1 Fluctuations in fusion plasmas

Nuclear fusion of light elements is the mechanism behind the energy generation in stars, and a successful fusion power plant promises clean and sustainable energy for the foreseeable future. However, controlling and harnessing the fusion process remains one of the greatest engineering challenges at present (and it has been — since the early 1950s). The process requires the fuel to have an exceedingly high temperature, which is therefore in the plasma state — an ionized gas. At the same time, the vessel containing the fuel should ideally be at room temperature or lower. Nowhere else on Earth are the temperature gradients as great, and maintaining this division of plasma fuel and material vessel is of critical importance for the sustained operation of a fusion power plant.

In the highly turbulent boundary region between the fusion plasma and material walls, relative fluctuations of order unity are ubiquitous. The problem of turbulence is one of the great remaining problems in classical physics. The highly complex and varied behaviour of turbulent fluids defy most attempts at simple and predictive description. In the boundary of fusion plasmas, the physical problem of turbulence meets the engineering challenge of fusion.

In this Chapter, I will briefly review the state of knowledge regarding fluctuations in the outer boundary of fusion plasmas. In Chapter 2, I will introduce a stochastic model capable of describing all statistical properties of these fluctuations, thereby providing a useful phenomenological model. The papers which are the main contribution of this thesis are summarized in Chapter 3, along with a list of my other published works. Chapter 4 concludes the thesis. Lastly the papers, where new predictions of the model are presented and the model is applied to measurement data from current fusion experiments, are presented.

1.1 Nuclear Fusion

At present, the main focus in the nuclear fusion community is on the process fusing deuterium (D) and tritium (T),

$$\mathrm{D} + \mathrm{T} \rightarrow \alpha + \mathrm{n} + 17.6\,\mathrm{MeV}, \tag{1.1}$$

resulting in an α-particle with kinetic energy of 3.5 MeV and a neutron (n) with kinetic energy 14.1 MeV [1]. This particular process has two main advantages. First, lighter elements provide larger energy gain per reaction, so using isotopes of the lightest element is favorable. Second, D-T fusion is the easiest process involving hydrogen isotopes to initiate, since it has the highest reaction rate at the lowest temperature. These isotopes are also relatively simple to access. Deuterium can be extracted from seawater, as roughly 0.015% of hydrogen is deuterium. Tritium is a radioactive isotope with a half-life of about 12 years, and must be obtained from breeding with the lithium isotope Li^6, which is obtainable from minerals found in the earth's crust.

Although D-T fusion is the easiest process of those involving hydrogen isotopes to initiate, it is by no means straightforward. For sustained fusion, temperatures of $10^8 - 10^9$ K are required. This guarantees that the fuel is not only gaseous, but also ionized, a plasma, which complicates containment. One way of containing a plasma is to use a magnetic field, as the motion of charged particles is strongly restricted in the plane perpendicular to the magnetic field, while they can move freely along magnetic field lines. Bending the field into a torus ensures particles moving only along the field never collide with the vessel walls. One of the most promising designs on this idea is the tokamak [1].

1.2 The tokamak concept

In Fig. 1.1, an illustration of the basic tokamak configuration is shown. Toroidal field coils around the vessel containing the plasma produce the main toroidal magnetic field. The central transformer then induces a toroidal plasma current, which both heats the plasma ohmically and sets up the primary poloidal magnetic field, establishing the equilibrium and plasma confinement by twisting the magnetic field into a helix shape. Unfortunately, the toroidal geometry induces forces which push the plasma radially outwards, towards the outer main walls of the toroidal vessel. Some of these forces are counteracted by the helical shape of the field, and some are counteracted by the field generated by the outer poloidal field coils, which in addition can be used to shape the plasma [1].

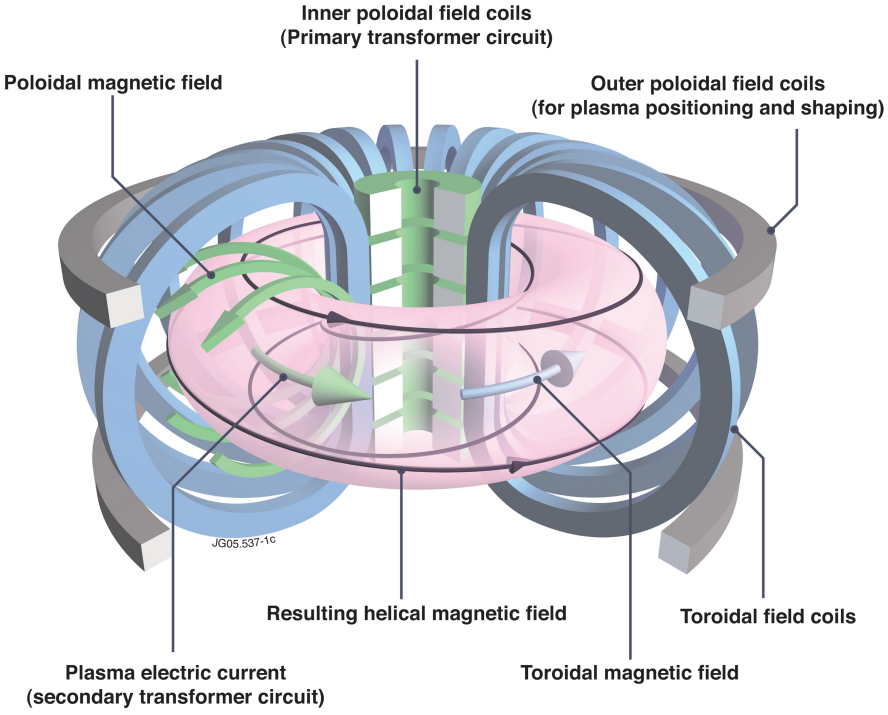

Figure 1.1: Illustration of a tokamak. Source: EUROfusion [2].

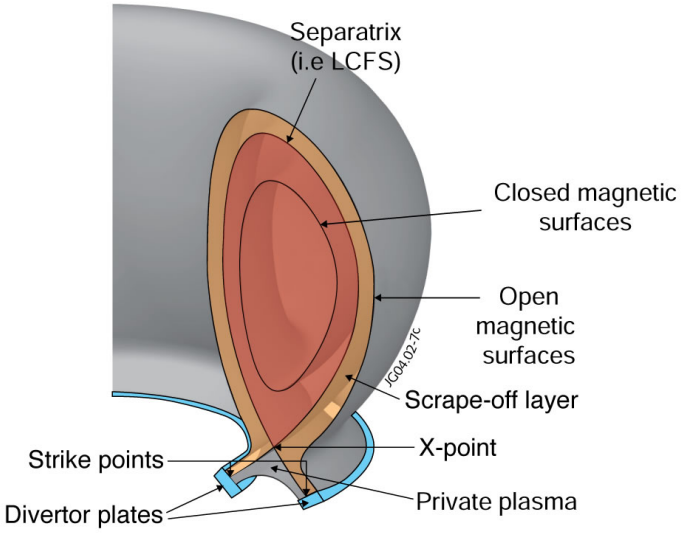

Figure 1.2: Illustration of the tokamak boundary region with a diverted magnetic field. Source: EUROfusion [2].

While an equilibrium is now established, the configuration must also handle both diffusive and turbulent cross-field transport. A divertor is usually introduced in order to address this transport. A cross-section of the divertor configuration is shown in Fig. 1.2 where the closed magnetic surfaces correspond to the magnetic surface seen in Fig. 1.1. The separatrix, or last closed flux surface (LCFS), separates the closed magnetic surfaces from those intersecting the divertor plates. The separatrix is associated to the X-point where the poloidal magnetic field vanishes. The region of open field surfaces intersecting the divertor plates is called the scrape-off layer (SOL), where the plasma drifting past the separatrix is transported down to the divertor plates. Due to the weak poloidal field near the X-point, the distance to the divertor plates along the magnetic field is very large, allowing plasma to cool before it contacts them. Further out, the magnetic field intersects limiter structures and components of the main vessel wall instead of the divertor, a region called the wall (or limiter) shadow. The intention is that particles entering the SOL from the confined plasma will move along field lines down to the divertor plates where their interactions with solid surfaces and their influence on the fusion process can be controlled, remote from the confined plasma column, instead of arriving at the main chamber wall, where they can damage sensitive equipment. Despite these efforts, it is found that the SOL plasma is highly turbulent with intermittent bursts of particle density and heat, leading to enhanced levels of plasma–surface interactions at the main chamber wall.

1.3 Plasma turbulence

In the most favourable case, the conditions at the LCFS and the wall would set the plasma density profile in the SOL and the radial transport in the SOL would be dominated by binary collisions and Fick's law of diffusive transport,

$$\Gamma_\perp = -D_\perp \frac{\partial n_\mathrm{e}}{\partial r}, \tag{1.2}$$

would be valid. Here, $\Gamma_\perp$ is the cross-field particle flux, n_e is the electron density, r is the radius and $D_\perp$ is the diffusivity, set by the flow conditions and the microscopic plasma behaviour. As cross-field diffusion is a slow process compared to particle motion along magnetic field lines, most of the plasma entering the SOL would arrive at the divertor targets.

In Figs. 1.3 and 1.4, radial profiles of the time-averaged electron density and other plasma parameters in the SOL are presented for various line-averaged particle densities $\bar{n}_\mathrm{e}$, a major experimental control parameter.[1] The variable

[1]The data set presented in Fig. 1.4 is from [3], and corresponds to the lowest and highest line averaged density shots from [4]. This data set is used in Figs. 1.4 and 1.7 in this thesis.

ρ in Fig. 1.3 is equivalent to $r - r_{\text{sep}}$ in Fig. 1.4, with 0 denoting the location of the LCFS and the rightmost dashed line (in both cases) indicating the transition to the wall shadow. The electron temperature T_e is approximately constant as a function of radius in the SOL and line-averaged density, see Fig. 1.3. The particle density and flux profiles, on the other hand, are strongly affected by the line-averaged density $\bar{n}_\text{e}$, or rather, the ratio between $\bar{n}_\text{e}$ and the discharge density limit n_G. While higher plasma density is beneficial for the fusion process, an empirical discharge density limit exists, defined as $n_\text{G} = (I_p/\pi a^2)10^{20}\,\text{m}^{-3}$, where I_p is the plasma current in units of mega-Amperes and a is the minor radius in units of meters. As this limit is approached, the probability of disruptions increases drastically [5, 6]. In both Figures, for low $\bar{n}_\text{e}$, the particle density profile decays sharply close to the LCFS, followed by a much slower decay radially outwards. The region of strong gradients is called the near-SOL, while the far-SOL is the region of weak gradients outside the near-SOL [7]. As $\bar{n}_\text{e}$ increases, the steep profile region moves to the left of the LCFS, and long decay lengths are seen throughout the SOL. This is consistent across numerous tokamak devices [3, 4, 7–15]. At the same time, the particle flux profile is nearly flat and increases with increasing line-averaged density. If the transport was diffusive with constant diffusion coefficient, this behaviour of the flux profile should be accompanied by an increasing density gradient, but the opposite happens. However, one can still estimate an effective diffusion coefficient, $D_\perp^\text{eff}$, from Eq. (1.2) using the measured profiles of n_e and $\Gamma_\perp$. This $D_\perp^\text{eff}$ varies by at least two orders of magnitude in Fig. 1.3, already indicating problems with the applicability of Eq. (1.2).

Additionally, comparing predictions for diffusion coefficients from classical cross-field diffusion to experimental values gives very poor agreement [16]. Empirical measurements of $D_\perp^\text{eff}$ are widely different in different experiments. In the JET, Alcator C-Mod and TCV tokamaks, the effective diffusion coefficient varies by several orders of magnitude as a function of radius through the SOL [3, 7, 16, 17]. In UEDGE transport simulations of the DIII-D tokamak, no diffusion coefficient could be chosen to fit experimental edge profiles [18]. In ESEL turbulence simulations of TCV SOL profiles and fluctuations, diffusion was unconvincing as an explanation for SOL transport, with strong radial variations in the estimated diffusion coefficient [3, 19].

One could try to add a convective term with some perpendicular velocity $V_\perp$,

$$\Gamma_\perp = -D_\perp \frac{\partial n_\text{e}}{\partial r} + V_\perp n_\text{e}. \tag{1.3}$$

This allows for a wide variety of particle density profiles [20], and UEDGE simulations could be fitted to DIII-D data for a single shot [18]. However, this model appears to have very poor predictive capabilities. In ESEL simulations

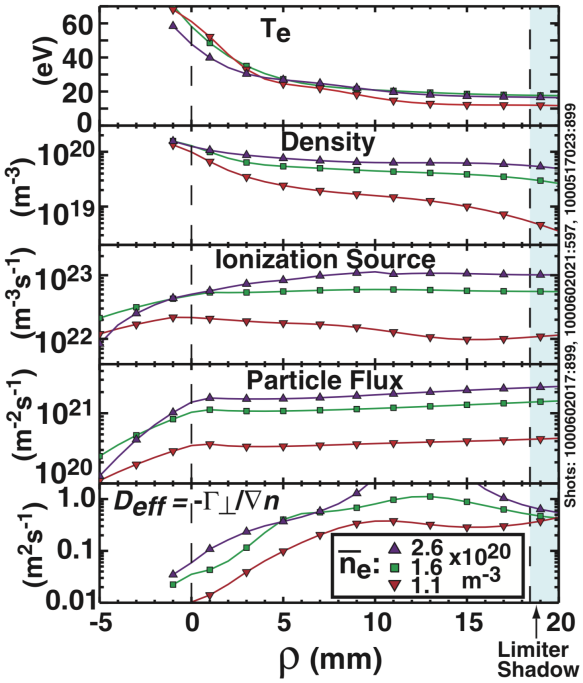

Figure 1.3: Radial profiles of electron temperature, particle density, ionization, particle flux and effective diffusion coefficient from Alcator C-Mod for various line-averaged densities. Reproduced from [6], © IOP Publishing. Reproduced with permission. All rights reserved. Originally appeared in [7], reproduced with the permission of AIP Publishing.

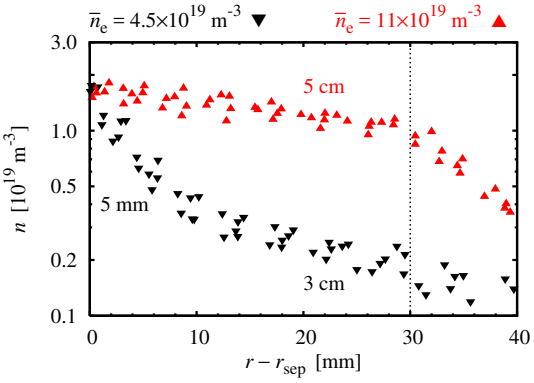

Figure 1.4: Radial electron density profiles from TCV for two different line-averaged densities. Image courtesy of O. E. Garcia.

of edge plasmas, no functional relationship on the form of Eq. (1.3) could be identified [3, 19], indicating that the diffusion–convection model may not be applicable to SOL plasmas either.

A different formalism is needed to understand SOL turbulence and describe the role of fluctuations in the plasma parameters. In order to arrive at such a formalism, it is necessary to review the current understanding of fluctuations in the SOL.

1.4 Intermittent fluctuations

Since the earliest measurements of fluctuations in the edge region of tokamaks, large relative fluctuation levels have been routinely observed. Levels of $10-90\%$ in the ion saturation current were seen in the Caltech tokamak [21, 22]. As seen in Fig. 1.5, relative particle density and floating potential fluctuations reach values above 0.5 in the TEXT device [23]. Here and for DIII-D in Fig. 1.6, $r/a > 0.8$ indicates the SOL and $r/a > 1$ is the wall shadow [23, 24]. More recent measurements of relative density fluctuation levels as a function of minor radius in the SOL of the TCV tokamak are shown in Fig. 1.7, corresponding to the average profiles presented in Fig. 1.4. The relative fluctuation level increases moderately outwards, but it does not appear to depend on the mean density. Relative fluctuation levels are above 0.5. Note that for the low density case, the relative fluctuation level increases sharply with radius in the near-SOL, compare Fig. 1.4. This indicates that the broad profiles in the far-SOL are connected to the large relative fluctuation level. These large relative fluctuation levels are in stark contrast to core turbulence, where relative fluctuation levels of only a few percent are observed. In Fig. 1.5, it is only for $r/a > 0.85$ that fluctuation levels become large. In Fig. 1.6, fluctuation analysis in the core is presented, showing that for $r/a < 0.85$, relative fluctuation levels are below 1% but this rises sharply into the SOL.

Visual inspection of fluctuation time series with high sampling rates from the SOL typically reveals that the large relative fluctuation levels are due to intermittent fluctuations with large positive bursts (and no apparent negative ones) that are asymmetric in time [7, 22, 25]. Recent experiments in the TCV, Alcator C-Mod and KSTAR tokamaks have been performed,[2] providing exceptionally long fluctuation data time series in the far-SOL at the outboard midplane. Excerpts from these time series are presented in Fig. 1.8, where

[2] All data sets are ion saturation current measured with electric probes. TCV indicates the data from Paper I. C-Mod indicates the dwell-probe data from the south-east electrode on the horizontal scanning probe during discharge 5 from [26]. KSTAR indicates the signal from the dwell-probe experiment in [27]. These data sets are used in Figs. 1.8, 1.15, 1.17, 1.19, 1.20 and 1.21 in this thesis.

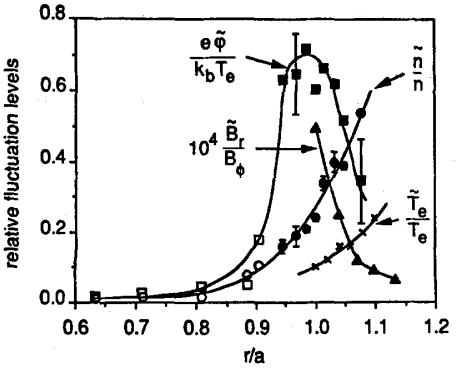

Figure 1.5: Fluctuation levels for various plasma parameters in the edge region in the TEXT tokamak measured by electric probes. Reproduced from [23], with the permission of AIP Publishing.

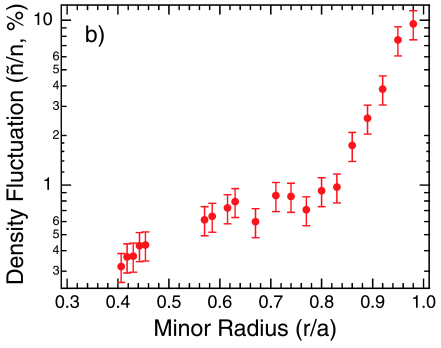

Figure 1.6: Fluctuation levels in the core and boundary of the DIII-D tokamak measured by beam emission spectroscopy. Reprinted from [24], with permission from JSPF.

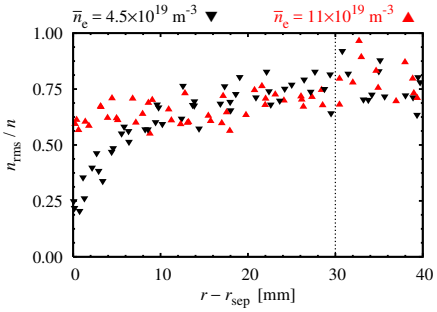

Figure 1.7: Edge fluctuations from TCV measured by electric probes. Image courtesy of O. E. Garcia.

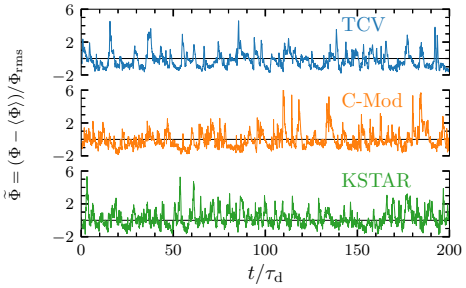

Figure 1.8: Excerpt of fluctuation time series from different devices. The solid black lines indicate the mean value.

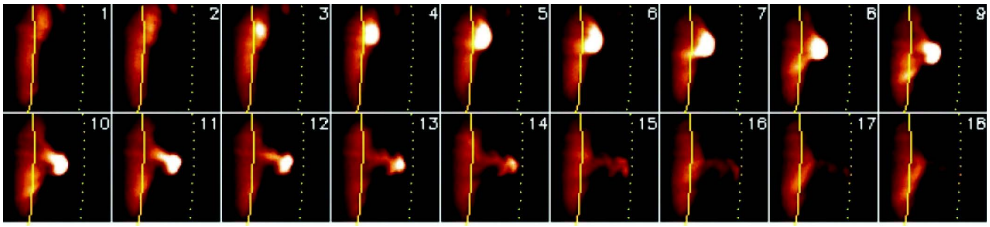

Figure 1.9: Sequence of a blob structure detaching from main plasma and moving through the SOL in NSTX. The full line shows the LCFS and the broken line shows the wall shadow. The frame rate is 7.5 μs/frame. Reproduced from [32], with the permission of AIP Publishing. Originally appeared in [33], reprinted with permission from Elsevier.

$\widetilde{\Phi}$ stands for the data time series Φ normalized by subtracting the mean and dividing by the rms-value. Here and in Figs. 1.17 and 1.19, time is normalized to the characteristic duration time of the large-amplitude bursts, τ_{d}. (How this parameter is estimated will be discussed in Chapter 2). In all cases, the fluctuations are strongly intermittent, with peak values frequently reaching 5 times the rms-value of the signal.

In order to further reveal the cause of these large-amplitude fluctuations, 2D-imaging of the SOL is required. During the late 1980's, using first 2D-probe arrays in the Caltech tokamak and then visible imaging with fast cameras in the TFTR tokamak, coherent structures, referred to as plasma blobs or filaments were observed in the SOL [28–31]. A more recent example of such a structure taken with GPI on NSTX is shown in Fig. 1.9. Here, a blob detaches from the main plasma and moves through the SOL, reaching the wall in about 100 μs. While some of the blob dissipates along the way, more plasma reaches the wall much faster than predicted from diffusive transport.

The blobs generally have a cross-field size of about 1 cm, radial velocity about 500 m/s and electron temperature in excess of 10 eV [32, 34, 35]. The blob size perpendicular to the magnetic field is smaller than but comparable to the SOL width ($\sim$ 5 cm), but much smaller than both machine size ($\sim$ 1 m) and magnetic connection length to the divertor plates ($\sim$ 10 m). Note that as plasma moves much more rapidly along the magnetic field than perpendicular to it, the blobs are elongated and field-aligned, as explicitly demonstrated by GPI in the poloidal-toroidal plane presented in Fig. 1.10. This field-aligned structure of the plasma blobs is also seen by fast-camera imaging on the MAST spherical tokamak [36, 37].

The blob structures are readily identified with the large-amplitude bursts seen in single-point time series from measurements in the SOL, as observed in

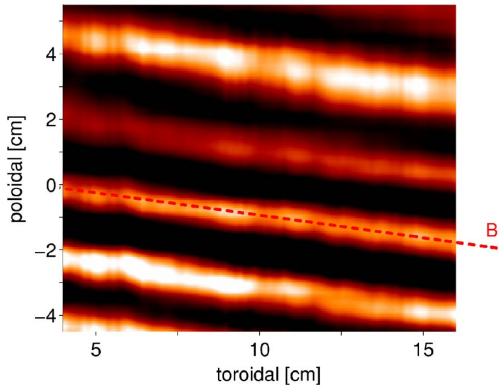

Figure 1.10: GPI from Alcator C-Mod showing the toroidal-poloidal cross-section of filaments. The red dashed line gives a magnetic field line. Reproduced from [38], with the permission of AIP Publishing.

Fig. 1.8. Each large-amplitude burst in the time series corresponds to a blob structure passing the probe. The asymmetric temporal structure is consistent with the sharp front and trailing wake of the filament seen in Fig. 1.9.

1.4.1 Motion of plasma filaments

Interchange motions have been identified as the mechanism for blob propagation [39]. An illustration of this mechanism is presented in Fig. 1.11. In the SOL on the outboard side, both the magnetic field curvature vector $\boldsymbol{\kappa}$ and gradient point radially inwards. Thus, both magnetic curvature and gradient particle drifts are downwards for ions and upwards for electrons. For a blob of excess pressure compared to the background plasma, this leads to charge polarization. The charge polarization sets up an internal electric field structure, leading in turn to a collective $\mathbf{E} \times \mathbf{B}$ drift, which drives the blob radially outwards. A snapshot of a simulated blob in motion is shown in Fig. 1.12. The polarization-induced electric dipole potential is also shown, with full lines indicating negative potential and broken lines indicating positive potential. These are the streamlines for the particle density, directed radially outwards at the peak amplitude of the blob structure [40–44].

Following the identification of the interchange mechanism, both simulations of individual blobs [40–42] and more general magnetized turbulence fluid simulations [46–48] were preformed. The ESEL model for the edge plasma [49, 50], incorporating both interchange motions and parallel losses, compared favorably to experimental measurements from the TCV SOL [3, 10]. The asymmetric burst structures observed in fluctuation time series are also present in

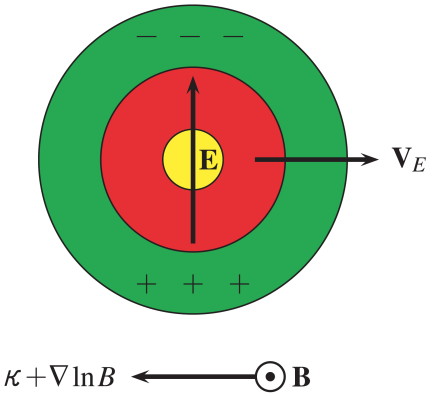

Figure 1.11: Illustration of the physical mechanism for the blob interchange motion. Reprinted from [45], with permission from JSPF.

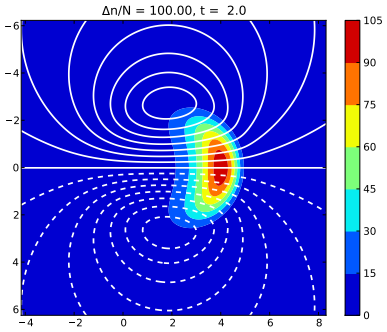

Figure 1.12: Simulation of blob with dipole potential. Image courtesy of O. E. Garcia and R. Kube.

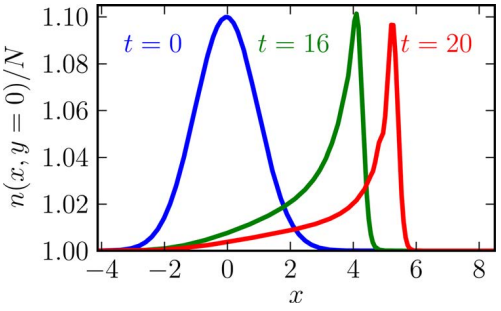

Figure 1.13: Simulation of blob developing front steepening as it travels. Reproduced from [43], with the permission of AIP Publishing.

these simulations of interchange motions in the SOL. In Fig. 1.13, the radial variation of the particle density of a simulated blob structure is plotted for different times [42, 43]. The blob structure develops a sharp front and a trailing wake, in qualitative agreement with the large–amplitude structures seen in Fig. 1.8 and the blob structure seen in Fig. 1.9.

While there are several other important aspects of blob motion and dynamics, such as scalings of velocities, correlation lengths or blob sizes with plasma parameters, how blobs connect to the divertor plates or how the blob structure along the magnetic field modifies its behaviour, the aspects I have reviewed are the ones most important to this thesis. See [32] for a review of SOL filaments.

1.4.2 Statistical properties

The SOL plasma fluctuations exhibit several statistical properties which appear universal across devices, plasma parameters and confinement modes. Analysis of relative fluctuation levels have been complimented by measurements of ion saturation current, particle density and temperature from a wide variety of devices, using electric probes and gas puff imaging (GPI), analysing probability density functions (PDFs) and frequency power spectra. The PDFs are found to be unimodal, positively skewed and flattened, and to have an exponential tail towards positive values [4, 11, 25, 45, 51, 52]. Examples from various devices are presented in Figs. 1.14 and Fig. 1.15. In Fig. 1.15, the black dashed line is the PDF predicted by the stochastic model presented in Chapter 2, given by Eq. (2.16). Due to the long duration of these particular data time series, exponential tails over 4 decades in probability are clearly seen in this Figure. The skewness and flatness moments for the signals presented in Fig. 1.14 were about 3 and 10, respectively, well in excess of values of 0 and 3, as expected for normally distributed signals. By comparison, the skewness and flatness moments for the signals presented in Fig. 1.15 were about 1.5 and 6 respectively, indicating a large range of variability in the intermittency of the fluctuations seen in the SOL for different plasma and machine parameters. Paper III discusses how the intermittency changes with radial position in the SOL of Alcator C-Mod, while the PDF in all cases is well described by a Gamma distribution. This distribution is derived in Paper V. Several different PDFs have been proposed to explain the fluctuations, some based on their similarity to experimental data and some based on phenomenological models, self-organized criticality (SOC) or properties of the fluctuations [52–60]. A parabolic relationship between the skewness and kurtosis moments was also reported, and its connection to the properties of the fluctuations and their PDFs has been explored [61–63].

In the frequency domain, the fluctuations show a remarkable similarity across devices [25, 64, 65]. In Figs. 1.16 and 1.17, some examples of frequency power spectral densities are presented, showing how the spectra measured in different devices collapse with the correct scaling of the frequency axis. In Fig. 1.16, λ is simply considered a scaling parameter. By contrast, in Fig. 1.17, τ_{d} is interpreted as the characteristic duration time of the large-amplitude bursts. The black dashed line gives the power spectral density for the stochastic model presented in Chapter 2, given by Eq. (2.19a). In all cases, there is a flat region for low frequencies, while for high frequencies the power spectrum decays according to a power law. In Paper III it is demonstrated that outside the LCFS in Alcator C-Mod, the shape of the frequency power spectrum and the value of τ_{d} are independent of the radial position and the ratio between the line averaged density and the empirical discharge density limit. They are also

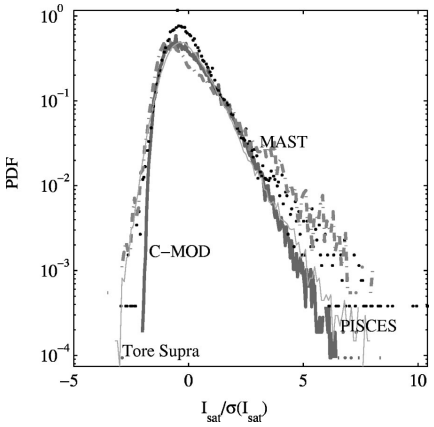

Figure 1.14: Skewed ion saturation current PDFs from the boundary region of various plasma confinement devices. Reproduced from [25], with the permission of AIP Publishing.

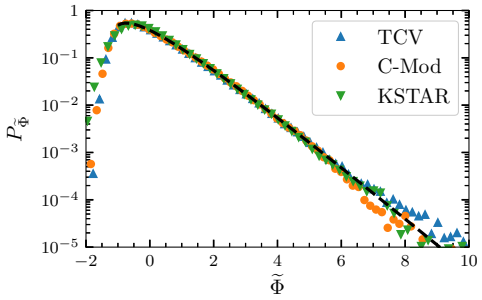

Figure 1.15: Amplitude probability density functions of the time series presented in Fig. 1.8. The broken line gives the prediction of the stochastic model.

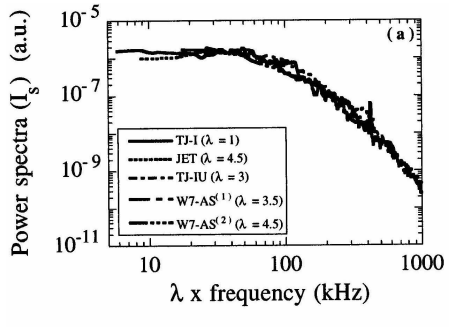

Figure 1.16: Ion saturation current power spectral densities from a variety of devices. Reprinted figure with permission from [64]. Copyright (1999) by the Americal Physical Society.

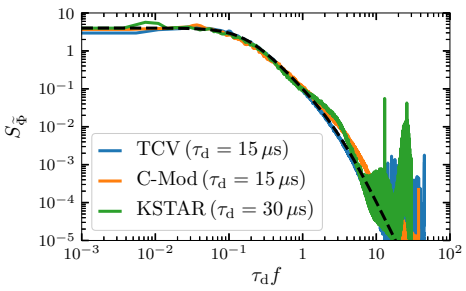

Figure 1.17: Power spectral densities of the time series presented in Figs. 1.8 and 1.15. The broken line gives the predicition of the stochastic model.

the same for several different confinement regimes in the far-SOL [66]. Due to the universal character and power-law tails of the frequency power spectra, they have previously been discussed in the context of self-organized criticality [25, 51, 64, 65].

In order to reveal the statistical properties of large-amplitude fluctuations, the conditional averaging technique is frequently used. A threshold value is chosen, taken to be 2.5 times the rms-value above the mean value by convention. Every time the signal crosses the threshold, a conditional window around the peak value of the signal is recorded. The average shape of the large-amplitude fluctuations is typically shown to be sharply peaked with a faster rise than decay [4, 11, 25–27, 35, 45, 51, 66–71], well fitted by exponential functions. The maximal amplitude of the conditional structures is shown to be very well exponentially distributed [26, 27, 35, 66, 71], and the waiting times between the peaks of the conditional structures are also exponentially distributed [26, 27, 35, 66, 69, 70, 72]. Some examples of conditionally averaged structures are presented in Figs. 1.18 and 1.19. In Fig. 1.18, results from conditional averaging of ESEL turbulence simulations are compared to conditional averaging of TCV particle density time series for various values of the line-averaged density. The conditional waveforms are similar for all line-averaged densities in the experiment, and the ESEL simulations compare favorably to the measurement data. In Fig. 1.19, conditional averaging of data time series for a variety of devices are presented together with an asymmetric, two-sided exponential function. The conditional waveforms are similar for all devices, and are in agreement with the two-sided exponential function. The conditional structures in both figures are consistent with the structure of a simulated blob, presented in Fig. 1.13. For the conditional structures presented in Fig. 1.19, the distribution of maximal amplitudes is presented in Fig. 1.20 and the distribution of the waiting time between these maxima is presented in Fig. 1.21. In both cases, the black dashed line gives an exponential decay. The distributions show a remarkable degree of similarity across devices, and the exponential decay is an excellent description of the distributions over two decades in probability.

These observations from conditional averaging, also presented in Paper I and Paper III, will be the input assumptions for the stochastic model. Before discussing the model, some comments on the importance of the intermittent SOL fluctuations for the operation of magnetically confined fusion power reactors are in order.

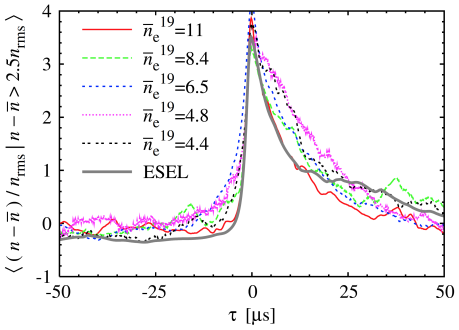

Figure 1.18: Comparison between conditional average of TCV particle density time series measured with an electrical probe and ESEL simulations. Reprinted from [4], with permission from IAEA.

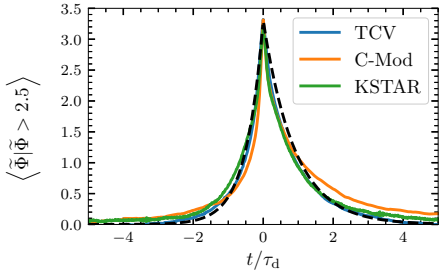

Figure 1.19: Conditionally averaged structures from the time series presented in Fig. 1.8. The broken line gives a two-sided exponential function.

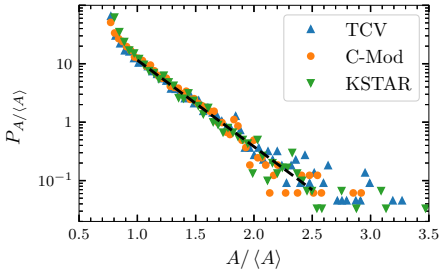

Figure 1.20: Distribution of maximal amplitude of conditionally averaged structures from the time series presented in Fig. 1.8. The broken line gives an exponential decay.

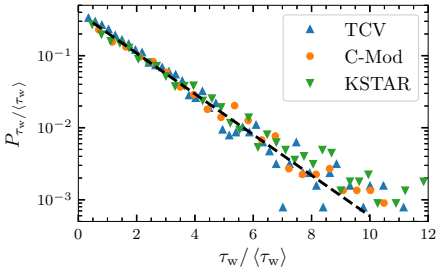

Figure 1.21: Waiting time distribution between conditionally averaged structures from the time series presented in Fig. 1.8. The broken line gives an exponential decay.

1.5 The importance of modelling fluctuations

While the SOL turbulence is an interesting physical problem in itself, and the models used to describe the turbulence may be applicable in several other physical systems characterised by intermittent fluctuations, see for example Refs. 1-10 in Paper II, the filamentary transport in the SOL is tied to a number of effects which are important for the operation of future fusion reactors.

As the line-averaged density approaches the discharge density limit, the profile in the far-SOL becomes gradually broader and flatter, see Figs. 1.3 and 1.4, leading to a marked increase in the particle density at the wall radius. At the same time, the relative fluctuation level remains constant, see Fig. 1.7, indicating an increased absolute fluctuation level as well. Both of these effects lead to a higher degree of plasma–wall interactions [3, 4, 7–15].

Here, I present an example of how the fluctuation level may influence the expected yield from physical sputtering. Physical sputtering depends on the particular species of the plasma ions and wall materials, as well as the energy of the incoming plasma particles. The number of sputtered particles per incoming particle is given by the modified Bohdansky yield function. Assuming for simplicity that plasma particles hit the target at a normal angle, it is given by [73]

$$Y(E) = QS_{\mathrm{n}}\left(\frac{E}{E_{\mathrm{TF}}}\right)\left[1-\left(\frac{E_{\mathrm{th}}}{E}\right)^{2/3}\right]\left(1-\frac{E_{\mathrm{th}}}{E}\right)^{2},\ E > E_{\mathrm{th}}, \tag{1.4}$$

and zero otherwise. Here, Q is the yield factor, E is the kinetic energy of the incoming ions, E_{TF} is the Thomas-Fermi energy, E_{th} is the threshold energy and S_{n} is the nuclear stopping cross section, given by

$$S_{\mathrm{n}}(x) = \frac{3.441\sqrt{x}\log(x+2.718)}{1+6.355\sqrt{x}+x(6.882\sqrt{x}-1.708)}. \tag{1.5}$$

For tungsten (W) walls and a deuterium (D) plasma, $Q = 0.07$, $E_{\mathrm{TF}} = 9925\,\mathrm{eV}$ and $E_{\mathrm{th}} = 209.37\,\mathrm{eV}$ [73]. The yield function is presented in Fig. 1.22 in the case where all incoming particles have equal energy, $E = \langle E\rangle$. It vanishes for $\langle E\rangle \leq E_{\mathrm{th}}$ and falls off for large $\langle E\rangle$ as the incoming particles have enough energy to penetrate deeper into the material instead of causing sputtering.

The simplest estimate for the impact energy of an ion of charge Z is $E = 2T_{\mathrm{i}} + 3ZT_{\mathrm{e}}$ [16, 73]. In the case of constant temperature, all incoming particles would impact the walls with the same energy, and any fluctuations in the particle density would not matter — only the average density would. This is not a realistic case, however, as the electron temperature in the SOL is highly correlated with the particle density fluctuations, and electron temperature near

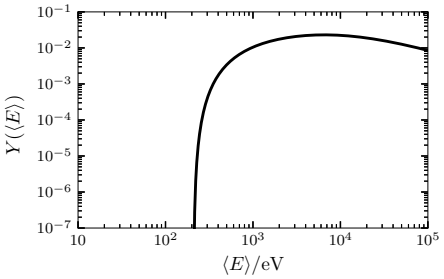

Figure 1.22: Yield function for D on W given by the modified Bohdansky formula.

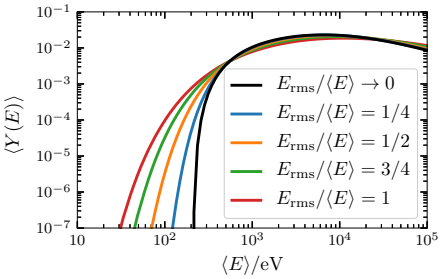

Figure 1.23: Mean yield function for D on W and for various values of the relative fluctuation level.

the wall of the Alcator C-Mod device closely follows a Gamma distribution [35]. Following [73], E is here assumed to follow a Gamma distribution. The mean sputtering yield is then given by

$$\langle Y(E)\rangle = \int_0^\infty Y(E)P_E(E)\mathrm{d}E = \int_{E_{\mathrm{th}}}^\infty Y(E)P_E(E)\mathrm{d}E, \tag{1.6}$$

where the second equality holds as $Y(E) = 0$ for $E < E_{\mathrm{th}}$.

In Fig. 1.23, the mean sputtering yield $\langle Y(E)\rangle$ as a function of $\langle E\rangle$ is presented for various values of the relative fluctuation level of the incoming ion energy E. The black curve given by $E_{\mathrm{rms}}/\langle E\rangle \to 0$ indicates the case where the relative fluctuation level is small enough for $\langle Y(E)\rangle \approx Y(\langle E\rangle)$ to hold and corresponds to the curve in Fig. 1.22. The main effect of the fluctuations is to allow for sputtering even if $\langle E\rangle < E_{\mathrm{th}}$, and in this case, the mean sputtering yield increases for increasing relative fluctuation level. This can also be seen from Eq. (1.6): Although the yield function vanishes for $E < E_{\mathrm{th}}$, $\langle Y(E)\rangle$ is always positive. For a given value of $\langle E\rangle$, increasing the relative fluctuation level gives access to higher energies, which increases $\langle Y(E)\rangle$ (at least for small $\langle E\rangle$).

This simple example shows one of the reasons why accurately describing the statistical properties of the fluctuating quantities is important: even if the measured average ion temperature is below a threshold where one would expect sputtering, there may still be a significant amount of sputtering if the fluctuations are sufficiently strong. This problem can be investigated in the reverse direction as well, asking how often the fluctuating quantity E crosses the threshold E_{th} and how long it typically remains above the threshold. This may be important for plasma–wall interactions, as some materials may better

handle short, intense bursts of energy than longer and weaker bursts and vice versa. The problem of finding the rate at which a signal crosses a threshold and the distribution of time spent above a threshold is called excess time statistics, and has been studied since the pioneering work by Rice [74, 75]. I will return to this problem in Sec. 2.4.

Several other effects may be linked to the filamentary turbulence. These include the broadening of the profiles, as well as plasma detaching from the divertor and the discharge density limit in itself [6, 7, 9, 14, 15]. Additionally, the filamentary structures may adversely affect radio-frequency wave heating [76–78]. A possible mechanism for relating blob transport to the density profiles is given in Sec. 2.5.1.

2 | Stochastic modelling

In this Chapter, I discuss a stochastic model used to describe the intermittent plasma fluctuations presented in the previous Chapter as a super-position of uncorrelated pulses. The model has been known for a long time [79], and was called the 'shot noise' model after it was used to describe noise in vacuum tubes [74, 75]. For reasons to become clear presently, I will call it the 'filtered Poisson process' (FPP). Over time, it has been successfully applied to a variety of systems in various scientific fields [80–86]. This model was first considered for SOL plasma fluctuations in 2012 [60], and it has since been applied for interpretation and description of probe and GPI measurements in the TCV (see Paper I), Alcator C-Mod (see Paper III), and KSTAR tokamaks, where all major assumptions and predictions of the model are shown to be consistent with the statistical properties of SOL fluctuations [26, 27, 35, 66, 69–71, 87].

I will briefly summarize the major results from the previous Chapter, and discuss how they are addressed by the model. Conditional averaging provides the assumptions for the model:

- Peaked and asymmetric conditionally averaged structures that are well described by a two-sided exponential function.
- The maximal amplitudes of the conditional structures are exponentially distributed.
- The waiting times between the maxima of conditional structures are exponentially distributed.

In the stochastic model, these structures reflect the blobs arriving at the probe / diode view position. The conditionally averaged structure and amplitude distribution reflects the shape and amplitude of the blobs and the waiting time distribution represents how blobs are separated in time and space. There are at least three experimental results which the model must reproduce:

- The parabolic relationship between the skewness and flatness moments.

- The unimodal, positively skewed and flattened probability distribution with an exponential tail for large amplitudes.
- The frequency power spectra which are flat for low frequencies and power-law-like for high frequencies.

As it turns out, the stochastic model predicts all of these properties. It furthermore predicts the excess time statistics to a high degree of accuracy. Three features of the SOL fluctuations are readily interpretable under the model:

- Relative fluctuation level increases from the LCFS through the SOL.
- Probability density functions are Gaussian-like near the LCFS and positively skewed and flattened in the far-SOL.
- The power spectral density has the same shape for all radial positions in the SOL.

Lastly, the radial particle density profiles have been explored using the model. I will present the simplest case in Sec. 2.5.1.

2.1 The filtered Poisson process

The stochastic model consists of a superposition of uncorrelated pulses, arriving according to a Poisson process. It is given on $t \in [0, T]$ by [60, 88]

$$\Phi(t) = \sum_{k=1}^{K(T)} A_k \varphi\left(\frac{t - t_k}{\tau_\mathrm{d}}, \lambda\right). \tag{2.1}$$

Here, Φ represents the time series under consideration, for example ion saturation current or GPI intensity. The pulse amplitudes A_k are independent and exponentially distributed with mean value $\langle A \rangle$. The pulse duration time is τ_d, and the pulse asymmetry parameter is given by λ. All pulses are assumed to be identical.

The number of pulses, $K(T)$ is taken to be Poisson distributed with intensity T/τ_w, where τ_w is the mean time between pulses,

$$P_K(K) = \frac{1}{K!}\left(\frac{T}{\tau_\mathrm{w}}\right)^K \exp\left(-\frac{T}{\tau_\mathrm{w}}\right). \tag{2.2}$$

Accordingly, the waiting times between consecutive pulses are independent and exponentially distributed with mean value τ_w and the arrival times t_k are independent and uniformly distributed on $[0, T]$ (strictly, K independent samples

of a uniform random variable U on $[0,T]$ are drawn, and the arrival times $t_1, t_2, \ldots, t_K$ are the ordered labels of $U_1, U_2, \ldots, U_K$) [89]. The motivation for using a Poisson process lies in its connection to the exponential waiting time distribution.

The pulse shape is taken to be an asymmetric, two-sided exponential function,

$$\varphi(\theta,\lambda) = \begin{cases} \exp\left(-\dfrac{\theta}{1-\lambda}\right), & \theta \geq 0, \\ \exp\left(\dfrac{\theta}{\lambda}\right), & \theta < 0, \end{cases} \tag{2.3}$$

where θ is a dimensionless variable and the asymmetry parameter λ is in the range $0 < \lambda < 1$. For $\lambda < 1/2$, the pulse has a faster rise than decay. In the following, setting $\lambda = 0$ indicates a one-sided exponential pulse shape,

$$\varphi(\theta,\lambda=0) = \begin{cases} \exp(-\theta), & \theta \geq 0, \\ 0, & \theta < 0. \end{cases} \tag{2.4}$$

This is consistent with taking the limit $\lim_{\lambda\to 0}\varphi(\theta,\lambda)$.

In order to calculate the moments and distribution of the process, the integrals

$$I_n = \int_{-\infty}^{\infty} \mathrm{d}\theta\, \varphi(\theta,\lambda)^n \tag{2.5}$$

are required. For the exponential pulse shape in Eq. (2.3), $I_n = 1/n$, independent of λ. This hints that the distribution and moments of Φ are independent of λ, a point I will return to.

This is the basic formulation of the process, incorporating all assumptions derived from conditional averaging of large–amplitude events. Note that in all cases, the statistically simplest applicable assumption has been made: All random variables are independent, the pulses are identical and there is no memory or correlations inherent in the process driving the system. The only further simplification would be to consider a one-sided exponential pulse, with the asymmetry parameter set to $\lambda = 0$. However, while experimentally estimated values of λ's are small, they are not negligible and the formulation with finite asymmetry is both necessary and, as will be evident, powerful.

The intensity is the defining parameter of the Poisson process, but it is not the most important parameter for our purposes as it provides a poor idea of how intermittent Φ appears. If the pulses are very narrow, even a high intensity results in a highly intermittent signal. Conversely, broad pulses quickly result in a slowly varying signal even for low intensities. The crucial parameter is

therefore the so-called *intermittency parameter* [60]

$$\gamma = \frac{\tau_{\mathrm{d}}}{\tau_{\mathrm{w}}}, \tag{2.6}$$

which gives a measure of how many new pulses one can typically expect during the life time of a single pulse. It therefore measures the degree of pulse overlap, where small values of γ gives a highly intermittent signal and large values of γ indicates a large degree of pulse overlap and a weakly intermittent signal.

2.1.1 The filtered Poisson process as a convolution

Equivalently to Eq. (2.1), the FPP can be written as a convolution. This is detailed in Paper II for $\lambda = 0$, but the result is valid for all pulse shapes φ,

$$\Phi(t) = \int_{-\infty}^{\infty} \mathrm{d}\theta \, \varphi\left(\frac{t}{\tau_{\mathrm{d}}} - \theta, \lambda\right) f_K(\theta) = \left[\varphi * f_K\right]\left(\frac{t}{\tau_{\mathrm{d}}}\right), \tag{2.7}$$

where

$$f_K(\theta) = \sum_{k=1}^{K(T)} A_k \delta\left(\theta - \frac{t_k}{\tau_{\mathrm{d}}}\right) \tag{2.8}$$

is a train of delta pulses. Thus, the FPP can be considered as either a superposition of uncorrelated pulses φ, or as a train of delta pulses filtered through φ. This justifies the name *filtered Poisson process*. If the pulse shape is known, Eq. (2.7) can in principle be deconvolved in order to find f_K, although this is difficult in practice. From f_K, the amplitudes A_k and arrival times t_k can be estimated directly. The first results from such calculations agree with the conclusions from conditional averaging and are presented in [87].

2.2 Moments and distribution

The first four moments of the FPP are given by [60]

$$\langle \Phi \rangle = \gamma \langle A \rangle I_1, \tag{2.9a}$$

$$\Phi_{\mathrm{rms}}^2 = \gamma \langle A^2 \rangle I_2, \tag{2.9b}$$

$$S_\Phi = \frac{1}{\gamma^{1/2}} \frac{\langle A^3 \rangle I_3}{\left(\langle A^2 \rangle I_2\right)^{3/2}}, \tag{2.9c}$$

$$F_\Phi = 3 + \frac{1}{\gamma} \frac{\langle A^4 \rangle I_4}{\left(\langle A^2 \rangle I_2\right)^2}. \tag{2.9d}$$

The relationship between skewness and flatness can therefore be given on the parabolic form

$$F_\Phi = 3 + \frac{\langle A^2\rangle\langle A^4\rangle}{\langle A^3\rangle^2}\frac{I_2 I_4}{I_3^2}S_\Phi^2. \tag{2.10}$$

Using that for the exponential pulse shape $I_n = 1/n$ and for the exponentially distributed amplitudes $\langle A^n\rangle = n!\langle A\rangle^n$, these expressions simplify to

$$\langle\Phi\rangle = \gamma\langle A\rangle, \tag{2.11a}$$

$$\Phi_{\text{rms}}^2 = \gamma\langle A\rangle^2, \tag{2.11b}$$

$$S_\Phi = \frac{2}{\gamma^{1/2}}, \tag{2.11c}$$

$$F_\Phi = 3 + \frac{6}{\gamma}, \tag{2.11d}$$

and accordingly [60, 88]

$$F_\Phi = 3 + \frac{3}{2}S_\Phi^2. \tag{2.12}$$

This expression provides the first required explanation: The universal parabolic relationship between the skewness and kurtosis moments. For the given pulse shape, this relationship is independent of λ. Because of the exponential distribution for the amplitudes, it is independent of $\langle A\rangle$. Different values of γ give different values of S_Φ and F_Φ, mapping out the parabolic relation. Thus, every realization of the process described by Eq. (2.1) gives a point on the parabola defined by Eq. (2.12), independent of the average amplitude or the pulse asymmetry.

The result that the FPP with $\lambda = 0$ follows a Gamma PDF with shape parameter γ and scale parameter $\langle A\rangle$ has been well known for a long time, and has been re-derived multiple times [90],

$$P_\Phi(\Phi) = \frac{\Phi^{\gamma-1}}{\langle A\rangle^\gamma\Gamma(\gamma)}\exp\left(-\frac{\Phi}{\langle A\rangle}\right),\ \Phi > 0. \tag{2.13}$$

Since this result can be derived using I_n, see for example Paper V, and I_n is independent of λ for the two-sided exponential function, it follows that the distribution is the same for *any* value of λ. For $\gamma > 1$, this provides the explanation for the unimodal, skewed and flattened probability distributions found in SOL plasmas. The intermittency parameter γ determines the shape of this distribution, and high γ leads to processes resembling normally distributed noise.

I also note that from Eqs. (2.11a) and (2.11b), the relative fluctuation level can be found:

$$\frac{\Phi_{\text{rms}}}{\langle\Phi\rangle} = \gamma^{-1/2}. \tag{2.14}$$

Thus, the increasing intermittency, the increasing relative fluctuation level and the gradually more skewed PDFs radially outward in the SOL are all reflected by decreasing γ. In GPI measurements from Alcator C-Mod (see Paper III and the next Section), τ_{d} remains constant through the SOL, suggesting that these observations all stem from the same source: an increasing τ_{w}, that is, fewer blobs are recorded in the far-SOL than in the near-SOL. This is likely due to stronger poloidal flows in the near-SOL leading to more blob overlap, combined with blob dispersion leading to less overlap in the far-SOL, see Paper III.

Using the normalization

$$\widetilde{\Phi} = \frac{\Phi - \langle \Phi \rangle}{\Phi_{\mathrm{rms}}} \tag{2.15}$$

provides a very useful form of Eq. (2.13):

$$P_{\widetilde{\Phi}}(\widetilde{\Phi}) = \frac{\gamma^{\gamma/2}}{\Gamma(\gamma)} \left(\widetilde{\Phi} + \gamma^{1/2} \right)^{\gamma-1} \exp\left(-\gamma^{1/2} \widetilde{\Phi} - \gamma \right), \; \widetilde{\Phi} > -\gamma^{1/2}. \tag{2.16}$$

In Fig. 1.15, this expression with $\gamma = 1.8$ is shown to be in agreement with the PDFs for experimental data time series from a variety of devices. I also note that the skewness and flatness moments calculated from Eqs. (2.11c) and (2.11d) with this γ-value are in agreement with the values of the moments reported in the text. This form of the distribution, along with the skewness and flatness moments, are independent of $\langle A \rangle$. Thus, they allow for reliably estimating the parameter γ from realizations of the process. For the fluctuation analysis, this is often far more important than estimating $\langle A \rangle$, as γ changes the character of the process while $\langle A \rangle$ simply scales the process. A reliable estimate of $\langle A \rangle$ is still desirable, as it is the only parameter directly related to the absolute value of the process. It may, however, not be physically meaningful in some experiments. In the case investigated in Paper I, the mean value of the signal was unreliable, as the diagnostic system was not capable of correctly measuring the low-frequency part of the signals. Before analysis, the signal had to be detrended. Even with a reliable estimate of γ from the normalized PDF of the signal, $\langle A \rangle$ could not be estimated. Neither do GPI measurements give a useful estimate of $\langle A \rangle$, as the GPI intensity is a nonlinear function of electron density, temperature and neutral gas density. Thus an estimate of $\langle A \rangle$ from the GPI intensity cannot be directly related to any of the plasma parameters.

The normalization in Eq. (2.15) provides two additional advantages. It is the natural normalization for the power spectral density and autocorrelation function, to be discussed in the following section. It is also readily extendable to normalizing the signal by a running average and running standard deviation,

in order to remove trends in the signals [26, 35]. This may be necessary, as Eq. (2.1) describes a statistically stationary process.

2.3 The power spectral density

The power spectral density can be found using the convolution form of Φ, given by Eq. (2.7). Then the inverse Fourier transform can be performed to find the auto-correlation function. The details can be found in Appendix B of Paper II for the case $\lambda = 0$. The generalization is straightforward. Since Φ is a pulse shape φ convolved with a pulse train f_K, the Fourier transform of Φ is the product of the Fourier transforms of the pulse shape and pulse train, and its power spectrum is the product of the power spectra of φ and f_K. As the delta pulse train has a flat power spectrum due to the uncorrelated pulses, the frequency dependence of the power spectrum and the time dependence of the autocorrelation function of Φ are given entirely by the pulse shape [91]:

$$S_\Phi(\omega) = \Phi_{\mathrm{rms}}^2 \frac{\tau_\mathrm{d}}{I_2} |\widehat{\varphi}(\tau_\mathrm{d}\omega)|^2 + 2\pi\tau_\mathrm{d}\langle\Phi\rangle^2 \delta\left(\tau_\mathrm{d}\omega\right), \tag{2.17a}$$

$$R_\Phi(t) = \Phi_{\mathrm{rms}}^2 \frac{1}{I_2} [\varphi * \varphi] \left(\frac{t}{\tau_\mathrm{d}}\right) + \langle\Phi\rangle^2, \tag{2.17b}$$

where ω is the angular frequency and

$$\widehat{\varphi}(\tau_\mathrm{d}\omega) = \int_{-\infty}^{\infty} \mathrm{d}\theta\, \varphi(\theta) \exp(-\mathrm{i}\theta\tau_\mathrm{d}\omega). \tag{2.18}$$

Using the normalization defined by Eq. (2.15), the dependence on the mean and rms–value disappears as well. Inserting the expression for the two-sided exponential pulse shape, Eq. (2.3), gives [92]

$$S_{\widetilde{\Phi}}(\omega) = \frac{2\tau_\mathrm{d}}{\left[1 + (1-\lambda)^2\tau_\mathrm{d}^2\omega^2\right]\left[1 + \lambda^2\tau_\mathrm{d}^2\omega^2\right]}, \tag{2.19a}$$

$$R_{\widetilde{\Phi}}(t) = \frac{1-\lambda}{1-2\lambda} \exp\left(-\frac{|t|}{(1-\lambda)\tau_\mathrm{d}}\right) - \frac{\lambda}{1-2\lambda} \exp\left(-\frac{|t|}{\lambda\tau_\mathrm{d}}\right). \tag{2.19b}$$

These expressions show that while the PDF is independent of λ, the power spectral density and auto-correlation function are independent of γ, that is, the degree of pulse overlap. This is due to the assumption of uncorrelated pulses. The power spectrum in Eq. (2.19a) is flat for low frequencies and falls off as ω^{-4} for high frequencies. If $\lambda = 0$ or $\lambda = 1$, the spectrum has a Lorentzian shape and falls as ω^{-2} instead. For small but finite λ, there is an

intermediate range where the spectrum falls as ω^{-2}, before rolling over to the ω^{-4} asymptote.

In Fig. 1.17, the expression in Eq. (2.19a) with $\lambda = 1/20$ compares favorably to the power spectral density from experimental data time series from a variety of devices. With $\lambda = 0$, the fit would be poor for the lowest three decades in power, supporting the notion that the parameter λ is a useful and important extension of to the model.

The FPP thus predicts a power spectrum which is flat for low frequencies and decays as either ω^{-2} or ω^{-4} for high frequencies. This is an excellent description of the power spectra seen in many different experimental contexts, and so provides the final required explanation: the shape of the power spectrum. Since the spectrum in Eq. (2.19a) is independent of γ, conditions leading to different degrees of intermittency play no role with respect to the power spectrum.

In GPI measurements from Alcator C-Mod (see Paper III), the power spectra were found to be independent of both radial position in the SOL and line-averaged density. Thus, both τ_{d} and λ were independent of radius and particle density. The model interpretation is that the blobs stabilize their shape quickly after formation, and keep this shape as they move through the SOL, irrespective of the line averaged density.

2.4 Excess time statistics

As seen in Sec. 1.5, threshold phenomena may demand the investigation of excess time statistics, such as how often a signal crosses a given threshold level, and how long the signal stays above the threshold. Excess time statistics has been investigated earlier, see for example Refs. 11-20 in Paper IV. First passage times have been discussed in the context of Ornstein–Uhlenbeck processes, which are equivalent to the normalized FPP in the limit $\gamma \to \infty$. For the FPP with $\lambda = 0$, the focus has mainly been on the rate of threshold crossings and the time below threshold. By allowing for $\lambda \neq 0$, the rate of threshold crossings provides an important diagnostic tool for parameter estimation, as well as providing interesting mathematical insight. Excess time statistics is discussed in detail in Paper IV.

The total number of threshold crossings is given by Rice's formula [75],

$$X(\Phi) = T \int_0^\infty \mathrm{d}\dot{\Phi}\dot{\Phi} P_{\Phi,\dot{\Phi}}(\Phi, \dot{\Phi}), \tag{2.20}$$

where $\dot{\Phi}$ is the derivative of Φ and $P_{\Phi,\dot{\Phi}}(\Phi, \dot{\Phi})$ is the joint PDF between Φ and its derivative. In order for a signal to cross the threshold Φ from below,

the signal must take on the value Φ and its derivative must be positive. The number of crossings per unit time is given by the integral in Eq. (2.20). The total number of threshold crossings $X(\Phi)$ is then the time duration of the process multiplied by this integral.

This expression presents a problem for many stochastic processes, particularly those based on white noise for randomness: the derivative of Φ does not necessarily exist, or have finite standard deviation. It also presents a problem for the standard formulation of the FPP with $\lambda = 0$: this process is not differentiable, as φ with $\lambda = 0$ is not. Other methods are applicable to the case of discontinuous pulses [85, 93]. This is where the formulation using finite λ is helpful, as the derivative of Φ exists in this case. For $\lambda \in (0, 1)$, the joint PDF between the process and its derivative can be formulated and Eq. (2.20) can be calculated. The details are given in Paper IV, and the result is

$$\frac{\tau_\mathrm{d}}{T} X(\Phi) = \frac{\lambda^{\gamma\lambda-1}(1-\lambda)^{\gamma(1-\lambda)-1}}{\gamma\Gamma(\gamma\lambda)\Gamma(\gamma(1-\lambda))} \left(\frac{\Phi}{\langle A\rangle}\right)^{\gamma} \exp\left(-\frac{\Phi}{\langle A\rangle}\right), \Phi > 0. \tag{2.21}$$

In this expression, the limit $\lambda \to 0$ can be taken, which gives the same results as calculations starting from $\lambda = 0$. While the functional form with respect to Φ depends on γ and $\langle A\rangle$, the prefactor depends on λ and τ_d as well as γ, meaning that this expression depends on all model parameters (if $\langle A\rangle$ cannot be reliably estimated, it can be removed by using the normalization in Eq. (2.15)). Thus, when the parameters have been estimated, the rate of threshold crossings provides an important consistency check on these parameters, as they do not only have to provide reasonable fits to PDF/moments and power spectrum separately, but at the same time provide a good fit to the rate of threshold crossings as well.

2.5 Extensions

The basic form of the FPP, Eq. (2.1) can be easily extended (although deriving closed analytical expressions for PDFs, power spectra and excess time statistics may be more difficult or impossible) by changing the amplitude distribution or the pulse shape. The radial velocity derived from the floating potential in probe measurements from TCV and Alcator C-Mod correspond well to the FPP with Laplace distributed amplitudes. This is demonstrated in Paper I and [35], and discussed in Paper V. Exponential frequency spectra have been observed in the edge region of magnetically confined plasmas, and may be connected to Lorentzian pulse shapes [94–97]. The FPP with Lorentzian pulses has been discussed in [91, 98, 99]. Other extensions include additive noise, discussed in Paper II, using different pulse shapes [92] or using randomly

distributed duration times [91, 92, 99]. Modifying the arrival time distribution is in general very difficult analytically, as this implies abandoning the Poisson process. However, a combination of Poisson-driven pulses and periodically arriving pulses may be applicable to for example thermal convection systems [100].

These extensions, however, only cover single-point measurements. By using a model for advection of single pulses, density profiles may be derived [88, 101–103].

2.5.1 Density profiles

The derivation presented here follows [88]. In order to arrive at an expression for the profiles, the FPP must be extended to cover both the radial direction (x) as well as time. It can be written as (fixing K for the moment)

$$\Phi_K(x,t) = \sum_{k=1}^{K} \phi_k(x,t). \tag{2.22}$$

Here, ϕ_k contains both the shape and the amplitude. Assuming the blobs do not interact [104] and follow an advection equation, their motion is given by

$$\frac{\partial \phi_k}{\partial t} + v_\perp \frac{\partial \phi_k}{\partial x} + \frac{\phi_k}{\tau_\parallel} = 0, \tag{2.23}$$

where $v_\perp$ is the constant radial velocity, and $\tau_\parallel$ describes losses along the magnetic field due to acoustic streaming. The solution to Eq. (2.23) is

$$\phi_k(x,t) = A_{0k} \exp\left(-\frac{t + x_k/v_\perp}{\tau_\parallel}\right) \varphi_k\left(\frac{x - x_k - v_\perp t}{l_\perp}\right), \tag{2.24}$$

where the k'th pulse has amplitude A_{0k} and is located at $x = 0$ at time $t_k = -x_k/v_\perp$, x_k is the position of the pulse at time $t = 0$, $l_\perp$ is the pulse size and $\varphi_k(\theta)$ is the spatial pulse shape. Setting a reference position ξ and letting $t_k = (\xi - x_k)/v_\perp$ be the time the pulse arrives at ξ, the process can be written as

$$\Phi_K(\xi,t) = \sum_{k=1}^{K} A_{0k} \exp\left(-\frac{\xi}{v_\perp \tau_\parallel} - \frac{t - t_k}{\tau_\parallel}\right) \varphi_k\left(-\frac{v_\perp}{l_\perp}\left[t - t_k\right]\right). \tag{2.25}$$

Letting the pulse shapes be identical one-sided exponential functions $\varphi_k = \exp(\theta)\Theta(-\theta)$, where Θ is the Heaviside function and $l_\perp$ is the blob size, the resulting process is

$$\Phi_K(\xi,t) = \sum_{k=1}^{K} A_{0k} \exp\left(-\frac{\xi}{v_\perp \tau_\parallel}\right) \exp\left(-\frac{t - t_k}{\tau_\mathrm{d}}\right) \Theta\left(\frac{t - t_k}{\tau_\mathrm{d}}\right). \tag{2.26}$$

where $\tau_\mathrm{d} = \tau_\parallel \tau_\perp / (\tau_\parallel + \tau_\perp)$ and $\tau_\perp = l_\perp / v_\perp$. This is equivalent to Eq. (2.1) with $A_k = A_{0k} \exp(-\xi / v_\perp \tau_\parallel)$ and the pulse shape in Eq. (2.4). The observed pulse duration time is the harmonic mean between parallel loss time and transit time past the probe, $\tau_\perp$. If the parallel loss time is very long, the pulse decay time seen by the probe is primarily set by the advection velocity. If the radial velocity is very low, $\tau_\perp$ is very long and the pulse decay seen by the probe is primarily due to parallel losses.

The radial profile is the average of this process, and can be written as

$$\langle \Phi \rangle(\xi) = \frac{\tau_\mathrm{d}}{\tau_\mathrm{w}} \langle A_0 \rangle \exp\left(-\frac{\xi}{v_\perp \tau_\parallel} \right), \tag{2.27}$$

In the case of fixed pulse size and velocity, the profile is an exponential function with decay length depending on the pulse velocity and the parallel loss time.

This can be further extended by allowing for varying (radially, temporarily and randomly distributed among pulses) velocities and pulse sizes, as well as for different parallel loss terms [102].

One limitation with this model is that the radial dependence on γ, that is the radial dependence on τ_w, is not seen. This is, however, a purely mathematical model, and pulses with arbitrarily small amplitudes still count towards the total number of pulses. Synthetic realizations of this process with a small amount of noise (or simply, where pulses with amplitudes below a threshold are removed) may be consistent with radially decreasing γ. Furthermore, it is a one-dimensional model only taking radial blob propagation into account. Other effects such as blob formation, two-dimensional motion in the plane perpendicular to the magnetic field and blob dispersion are not part of the model.

3 | Summary of Papers

The main focuses of the papers presented here are theoretical advances on the stochastic model and on methods for analysing fluctuation data time series. These comprise three of the included papers. In addition, two of the papers apply this analysis to plasma fluctuations in the SOL for Alcator C-Mod and TCV.

Paper I presents an analysis of Langmuir probe data from TCV. The probe was dwelled by the outboard mid-plane wall for 1 second, providing long, stationary data time series. This paper helps in justifying the stochastic modelling perspective and uses PDFs, conditional averaging and auto-correlation functions to achieve this aim. While the ion saturation current signal is the main signal of interest, floating potential, particle flux and radial velocity estimated from the floating potential are also considered. The radial velocity, in particular, appears amenable to continued stochastic modelling as the PDF is well described by the FPP with exponential pulse shapes and Laplace distributed amplitudes. (Note that this PDF, described in Eq. (40) in Paper V, is of the same form as the PDF for the derivative of the FPP, described by Eq. (24) Paper IV).

Noise is often present in experimental contexts, and affects the PDF, frequency power spectrum and excess time statistics of data time series, as in Paper III. The role of additive, normally distributed noise is addressed in Paper II. The noise affects the moments and PDF by bringing the PDF of the FPP with noise closer to a normal distribution, particularly for small values of the random variable. The noise breaks the non-negative property of the signal for positive definite amplitudes of the FPP, which suggests that a normal distribution may not be the best description of the noise, as both ion saturation current and GPI intensity are positive definite. The presence of a background density may alleviate this. The frequency power spectrum is also calculated and described. If the noise has the same autocorrelation function as the FPP, the power spectrum is unaffected. If the noise is delta-correlated, the high-frequency tail of the power spectrum rises and flattens, and the flat part

for low frequencies decreases in value. Methods for parameter estimation for the FPP with additive noise are studied using Monte-Carlo simulations. The results in this paper are general, and applicable to systems outside the SOL of fusion plasmas.

In Paper III (a letter), GPI data from ohmically heated plasmas in Alcator C-Mod is analysed for different line-averaged densities. In all cases, PDFs become less Gaussian as the limiter shadow region is approached from the LCFS. This increase in intermittency through the SOL is consistent with the increased relative fluctuation level. Thus, the pulse overlap decreases through the SOL, signifying that pulses are depleted and dissipate as they move. Line averaged density does not appear to significantly alter the number of blobs. At the same time, conditionally averaged pulse shapes and power spectra remain basically constant with both changing radial position and line averaged density. Under the stochastic model, the interpretation is that the blobs quickly take on their shape as they are formed, that this shape is unaffected by the plasma density, and that this shape remains constant as the blobs propagate through the scrape-off layer. The stochastic model describes the fluctuations at all radial positions in the SOL; PDFs, power spectra and rates of level crossings are consistent with the stochastic model.

The last two papers deal with some theoretical aspects of the FPP, and the results may be applied to other physical systems. Paper IV deals with level crossings and excess time statistics. Several authors have previously investigated the rate of threshold crossings for the FPP, but require a one-sided exponential function. By using the two-sided exponential pulse, Rice's formula may be applied directly. The rate of threshold crossings conforms to the rate for the one-sided pulse in the correct limit. While the pulse asymmetry λ does not enter into the expression for the PDF (as it does not enter I_n), it does enter the expression for the rate of threshold crossings. Thus the rate of threshold crossings depends on all parameters of the process, $\langle A \rangle$, τ_d, γ and λ, and provides an option for parameter estimation or a consistency check for the values of τ_d and λ found from conditional averaging or the power spectrum and γ and $\langle A \rangle$ from the moments or PDF. This contribution also contains analytical expressions for the distribution of time spent above threshold in the limits of weak and strong intermittency, and numerical results bridging the gap between these for intermediate intermittency levels.

Finally, Paper V contains results related to the effect of the pulse amplitude distribution on the distribution of the FPP. Exponentially distributed pulse amplitudes results in a Gamma distribution, which gives a good description of the ion saturation current, GPI intensity and temperature fluctuations in the SOL of fusion plasmas. One might ask how much the large amplitudes

contribute compared to the small amplitudes which, for the exponential distribution, are far more numerous. The comparison to a Gamma distribution with shape parameter greater than unity is natural, as this distribution has an exponential tail, but falls to zero for small values of the random variable. It turns out that the PDF of the FPP with Gamma distributed amplitudes with shape parameter 2 can be expressed analytically. This PDF is, however, very close to the PDF of the FPP with exponentially distributed amplitudes and slightly higher intermittency parameter. This indicates that the low amplitude events do not significantly alter the shape of the PDF. The PDF of the FPP with Laplace distributed amplitudes is derived, providing the origin of the expressions used for the radial velocity in Paper I and [35]. While more general amplitude distributions, such as the Gamma distribution with arbitrary shape parameter or the skewed Laplace distribution, may be of interest, analytical expressions for the PDF of the FPP only exist in special cases. This is particularly true if additive noise is also considered. By contrast, the characteristic function is often available. Therefore, a numerical study of parameter estimation from the characteristic function is also performed in this contribution.

3.1 List of other works

I am a co-author of several other publications, and I have some conference presentations. These are detailed in the following list:

Unpublished manuscripts

G. Decristoforo, O. E. Garcia, R. Kube and A. Theodorsen: 'Intermittent fluctuations and Lorentzian pulses in flux-driven thermal convection', in preparation. [100]

A. Theodorsen, O. E. Garcia, R. Kube, B. LaBombard and J. L. Terry: 'Universality of Poisson-driven plasma fluctuations in the Alcator C-Mod scrape-off layer', ready for submission, arXiv: 1802.05052. [87]

2018

R. Kube, O. E. Garcia, A. Theodorsen, D. Brunner, A. Kuang, B. LaBombard, J. L. Terry: 'Intermittent electron density and temperature fluctuations and associated fluxes in the Alcator C-Mod scrape-off layer', Plasma Physics and Controlled Fusion 60, 065002. [35]

O. E. Garcia, R. Kube, A. Theodorsen, B. LaBombard and J. L. Terry: 'Intermittent fluctuations in the Alcator C-Mod scrape-off layer for ohmic and high confinement mode plasmas', Physics of Plasmas 25, 056103. [66]

O. E. Garcia and A. Theodorsen: 'Intermittent fluctuations due to uncorrelated Lorentzian pulses', Physics of Plasmas 25, 014506. [99]

O. E. Garcia and A. Theodorsen: 'Skewed Lorentzian pulses and exponential frequency power spectra', Physics of Plasmas 25, 014503. [98]

2017

O. E. Garcia and A. Theodorsen, 'Auto-correlation function and frequency spectrum due to a super-position of uncorrelated exponential pulses', Physics of Plasmas 24, 032309. [92]

O. E. Garcia and A. Theodorsen, 'Power law spectra and intermittent fluctuations due to uncorrelated Lorentzian pulses', Physics of Plasmas 24, 020704. [91]

O. E. Garcia, R. Kube, A. Theodorsen, J.-G. Bak, S.-H. Hong, H.-S. Kim, the KSTAR Project Team and R. A. Pitts, 'SOL width and intermittent fluctuations in KSTAR', Nuclear Materials and Energy 12, 36-43. [27]

2016

O. E. Garcia, R. Kube, A. Theodorsen and H. L. Pécseli, 'Stochastic modelling of intermittent fluctuations in the scrape-off layer: Correlations, distributions, level crossings and moment estimation', Physics of Plasmas 23, 052308. [88]

A. Theodorsen and O. E. Garcia, 'Level crossings, excess times, and transient plasma-wall interactions in fusion plasmas', Physics of Plasmas 23, 040702. [105]

R. Kube, A. Theodorsen, O. E. Garcia, B. LaBombard and J. L. Terry, 'Fluctuation statistics in the scrape-off layer of Alcator C-Mod', Plasma Physics and Controlled Fusion 58, 054001. [26]

Oral Conference Presentations

2017

A. Theodorsen, O. E. Garcia, R. Kube, B. LaBombard and J. L. Terry: 'Application of RL-deconvolution for identifying burst amplitudes and arrival times in Alcator C-Mod far SOL plasma fluctuations'. Contributed oral presentation, 59th Annual Meeting of the APS Division of Plasma Physics. Session CO4.12

A. Theodorsen and O. E. Garcia: 'Using statistics to describe turbulence in fusion plasmas'. Invited award talk for Martin Landrøs prize, Fysikermøtet i Tromsø. Program

2016

A. Theodorsen, O. E. Garcia, R. Kube, D. Brunner, B. LaBombard and J. L. Terry: 'Level crossings and excess times of intermittent fluctuations in scrape-off layer plasmas'. Contributed oral presentation, 58th Annual Meeting of the APS Division of Plasma Physics. Session UO4.2

4 | Conclusion and future work

The implications of turbulent fluctuations in the boundary of fusion plasmas is a serious concern for the next generation confinement experiments and future fusion power reactors. As such, an accurate description of all the statistical properties of the turbulence is a necessary first step for both understanding and predicting its causes and effects on the reactor and walls. The filtered Poisson process is capable of describing the fluctuation probability densities, power spectra, level crossing rates and possibly the radial profiles observed in the scrape-off layer. In this thesis, the stochastic model has been extended by considering the effect of normally distributed noise and different amplitude distributions and by providing predictions for excess time statistics. The excess time predictions are consistent with GPI data in Alcator C-Mod. Additionally, the assumptions of the model have been tested on Langmuir probe data from TCV and on GPI data from Alcator C-Mod. The universal shape of the power spectral density of fluctuations in Alcator C-Mod has been interpreted using the model.

Future work will involve analysis of experimental data and numerical simulations as well as theoretical work extending the model. By analysing scans in plasma parameters such as plasma current, particle density, magnetic field strength or SOL width, scalings of model parameters can be discovered. The universality of the fluctuations can also be investigated by comparing tokamaks, spherical tokamaks and stellarators with different machine parameters, and in different confinement regimes.

The model provides a powerful tool for code validation, as numerical simulations of SOL turbulence must replicate the fluctuation statistics described by the model. In addition, scaling of particle and heat transport with model parameters, as well as the role of the SOL width and the effects of the boundary conditions, can be investigated using numerical simulations.

While some work on the correlations between ion saturation current, temperature, floating potential and radial velocity has already been performed, the model has not yet been extended to describe multiple, correlated, variables.

The different fluxes, computable from the time series of different plasma variables, should also be investigated using the model. In addition, the possible role of low-frequency trends, multiple temporal scales and clustering of events can be explored. The method for deconvolving data time series with the pulse shape in order to reveal the underlying pulse amplitudes and arrival times is still in its infancy. Monte-Carlo studies assessing the role of pulse overlap and additive noise and optimization for long time series is necessary before the method can be applied systematically.

Bibliography

[1] J. P. Freidberg, *Plasma Physics and Fusion Energy* (Cambridge University Press, Cambridge, 2007).

[2] "EUROfusion," https://www.euro-fusion.org.

[3] O. E. Garcia, R. A. Pitts, J. Horacek, A. H. Nielsen, W. Fundamenski, J. P. Graves, V. Naulin, and J. J. Rasmussen, J. Nucl. Mater. **363-365**, 575 (2007).

[4] O. E. Garcia, J. Horacek, R. A. Pitts, A. H. Nielsen, W. Fundamenski, V. Naulin, and J. J. Rasmussen, Nucl. Fusion **47**, 667 (2007).

[5] M. Greenwald, J. L. Terry, S. M. Wolfe, S. Ejima, M. G. Bell, S. M. Kaye, and G. H. Neilson, Nucl. Fusion **28**, 2199 (1988).

[6] M. Greenwald, Plasma Phys. Control. Fusion **44**, 201 (2002).

[7] B. LaBombard, R. L. Boivin, M. Greenwald, J. Hughes, B. Lipschultz, D. Mossessian, C. S. Pitcher, J. L. Terry, S. J. Zweben, and Alcator Group, Phys. Plasmas **8**, 2107 (2001).

[8] D. L. Rudakov, J. A. Boedo, R. A. Moyer, P. C. Stangeby, J. G. Watkins, D. G. Whyte, L. Zeng, N. H. Brooks, R. P. Doerner, T. E. Evans, M. E. Fenstermacher, M. Groth, E. M. Hollmann, S. I. Krasheninnikov, C. J. Lasnier, A. W. Leonard, M. A. Mahdavi, G. R. McKee, A. G. McLean, A. Y. Pigarov, W. R. Wampler, G. Wang, W. P. West, and C. P. C. Wong, Nucl. Fusion **45**, 1589 (2005).

[9] B. LaBombard, J. W. Hughes, D. Mossessian, M. Greenwald, B. Lipschultz, J. L. Terry, and the Alcator C-Mod Team, Nucl. Fusion **45**, 1658 (2005).

[10] O. E. Garcia, J. Horacek, R. A. Pitts, A. H. Nielsen, W. Fundamenski, J. P. Graves, V. Naulin, and J. J. Rasmussen, Plasma Phys. Control. Fusion **48**, L1 (2006).

[11] O. E. Garcia, R. A. Pitts, J. Horacek, J. Madsen, V. Naulin, A. H. Nielsen, and J. J. Rasmussen, Plasma Phys. Control. Fusion **49**, B47 (2007).

[12] F. Militello, P. Tamain, W. Fundamenski, A. Kirk, V. Naulin, and A. H. Nielsen, Plasma Phys. Control. Fusion **55**, 025005 (2013).

[13] J. A. Boedo, J. R. Myra, S. J. Zweben, R. Maingi, R. J. Maqueda, V. A. Soukhanovskii, J. W. Ahn, J. Canik, N. Crocker, D. A. D'Ippolito, R. E. Bell, H. Kugel, B. Leblanc, L. A. Roquemore, and D. L. Rudakov, Phys. Plasmas **21**, 042309 (2014).

[14] D. Carralero, G. Birkenmeier, H. W. Müller, P. Manz, P. DeMarne, S. H. Müller, F. Reimold, U. Stroth, M. Wischmeier, and E. Wolfrum, Nucl. Fusion **54**, 123005 (2014).

[15] D. Carralero, P. Manz, L. Aho-Mantila, G. Birkenmeier, M. Brix, M. Groth, H. W. Müller, U. Stroth, N. Vianello, and E. Wolfrum, Phys. Rev. Lett. **115**, 215002 (2015).

[16] P. C. Stangeby, *The Plasma Boundary of Magnetic Fusion Devices*, Series in Plasma Physics (CRC Press, 2000).

[17] B. Lipschultz, B. LaBombard, C. S. Pitcher, and R. L. Boivin, Plasma Phys. Control. Fusion **44**, 309 (2002).

[18] A. Y. Pigarov, S. I. Krasheninnikov, T. D. Rognlien, M. J. Schaffer, and W. P. West, Phys. Plasmas **9**, 1287 (2002).

[19] V. Naulin, J. Nucl. Mater. **363-365**, 24 (2007).

[20] P. C. Stangeby, Phys. Plasmas **9**, 3489 (2002).

[21] S. J. Zweben, P. C. Liewer, and R. W. Gould, J. Nucl. Mater. **111-112**, 39 (1982).

[22] S. J. Zweben and R. W. Gould, Nucl. Fusion **23**, 1625 (1983).

[23] A. J. Wootton, B. A. Carreras, H. Matsumoto, K. McGuire, W. A. Peebles, C. P. Ritz, P. W. Terry, and S. J. Zweben, Phys. Fluids B Plasma Phys. **2**, 2879 (1990).

[24] G. R. McKee, R. J. Fonck, D. K. Gupta, D. J. Schlossberg, M. W. Shafer, R. L. Boivin, and W. Solomon, Plasma Fusion Res. **2**, S1025 (2007).

[25] G. Y. Antar, G. Counsell, Y. Yu, B. Labombard, and P. Devynck, Phys. Plasmas **10**, 419 (2003).

[26] R. Kube, A. Theodorsen, O. E. Garcia, B. LaBombard, and J. L. Terry, Plasma Phys. Control. Fusion **58**, 054001 (2016).

[27] O. E. Garcia, R. Kube, A. Theodorsen, J.-G. Bak, S.-H. Hong, H.-S. Kim, the KSTAR Project Team, and R. A. Pitts, Nucl. Mater. Energy **12**, 36 (2017).

[28] S. J. Zweben, Phys. Fluids **28**, 974 (1985).

[29] S. J. Zweben and R. W. Gould, Nucl. Fusion **25**, 171 (1985).

[30] S. J. Zweben, D. Manos, R. V. Budny, P. Efthimion, E. Fredrickson, H. Greenside, K. W. Hill, S. Hiroe, S. Kilpatrick, K. McGuire, S. S. Medley, H. K. Park, A. T. Ramsey, and J. Wilgen, J. Nucl. Mater. **145-147**, 250 (1987).

[31] S. J. Zweben and S. S. Medley, Phys. Fluids B Plasma Phys. **1**, 2058 (1989).

[32] D. A. D'Ippolito, J. R. Myra, and S. J. Zweben, Phys. Plasmas **18**, 060501 (2011).

[33] R. J. Maqueda, D. P. Stotler, and S. J. Zweben, J. Nucl. Mater. **415**, S459 (2011).

[34] R. Kube, O. E. Garcia, B. LaBombard, J. L. Terry, and S. J. Zweben, J. Nucl. Mater. **438**, S505 (2013).

[35] R. Kube, O. E. Garcia, A. Theodorsen, D. Brunner, A. Q. Kuang, B. LaBombard, and J. L. Terry, Plasma Phys. Control. Fusion **60**, 065002 (2018).

[36] A. Kirk, N. B. Ayed, G. Counsell, B. Dudson, T. Eich, A. Herrmann, B. Koch, R. Martin, A. Meakins, S. Saarelma, R. Scannell, S. Tallents, M. Walsh, H. R. Wilson, and the MAST Team, Plasma Phys. Control. Fusion **48**, B433 (2006).

[37] N. Ben Ayed, A. Kirk, B. Dudson, S. Tallents, R. G. L. Vann, and H. R. Wilson, Plasma Phys. Control. Fusion **51**, 035016 (2009).

[38] O. Grulke, J. L. Terry, B. LaBombard, and S. J. Zweben, Phys. Plasmas **13**, 012306 (2006).

[39] S. I. Krasheninnikov, Phys. Lett. A **283**, 368 (2001).

[40] N. H. Bian, S. Benkadda, J.-V. Paulsen, and O. E. Garcia, Phys. Plasmas **10**, 671 (2003).

[41] O. E. Garcia, N. H. Bian, V. Naulin, A. H. Nielsen, and J. J. Rasmussen, Phys. Plasmas **12**, 090701 (2005).

[42] O. E. Garcia, N. H. Bian, and W. Fundamenski, Phys. Plasmas **13**, 082309 (2006).

[43] R. Kube and O. E. Garcia, Phys. Plasmas **18**, 18 (2011).

[44] R. Kube and O. E. Garcia, Phys. Plasmas **19**, 042305 (2012).

[45] O. E. Garcia, Plasma Fusion Res. **4**, 019 (2009).

[46] O. E. Garcia, N. H. Bian, J.-V. Paulsen, S. Benkadda, and K. Rypdal, Plasma Phys. Control. Fusion **45**, 919 (2003).

[47] O. E. Garcia and N. H. Bian, Phys. Rev. E **68**, 047301 (2003).

[48] O. E. Garcia, N. H. Bian, V. Naulin, A. H. Nielsen, and J. J. Rasmussen, Phys. Scr. **T122**, 104 (2006).

[49] O. E. Garcia, V. Naulin, A. H. Nielsen, and J. J. Rasmussen, Phys. Rev. Lett. **92**, 165003 (2004).

[50] O. E. Garcia, V. Naulin, A. H. Nielsen, and J. J. Rasmussen, Phys. Scr. **2006**, 89 (2006).

[51] G. Y. Antar, P. Devynck, X. Garbet, and S. C. Luckhardt, Phys. Plasmas **8**, 1612 (2001).

[52] J. P. Graves, J. Horacek, R. A. Pitts, and K. I. Hopcraft, Plasma Phys. Control. Fusion **47**, L1 (2005).

[53] B. A. Carreras, C. Hidalgo, E. Sánchez, M. A. Pedrosa, R. Balbín, I. García-Cortés, B. van Milligen, D. E. Newman, and V. E. Lynch, Phys. Plasmas **3**, 2664 (1996).

[54] B. A. Carreras, B. van Milligen, C. Hidalgo, R. Balbín, E. Sanchez, I. Garcia-Cortes, M. A. Pedrosa, J. Bleuel, and M. Endler, Phys. Rev. Lett. **83**, 3653 (1999).

[55] F. Sattin, N. Vianello, and M. Valisa, Phys. Plasmas **11**, 5032 (2004).

[56] B. P. van Milligen, R. Sánchez, B. A. Carreras, V. E. Lynch, B. LaBombard, M. A. Pedrosa, C. Hidalgo, B. Gonçalves, and R. Balbín, Phys. Plasmas **12**, 052507 (2005).

[57] J. M. Dewhurst, B. Hnat, N. Ohno, R. O. Dendy, S. Masuzaki, T. Morisaki, and A. Komori, Plasma Phys. Control. Fusion **50**, 095013 (2008).

[58] E.-J. Kim and J. Anderson, Phys. Plasmas **15**, 114506 (2008).

[59] J. Anderson and P. Xanthopoulos, Phys. Plasmas **17**, 110702 (2010).

[60] O. E. Garcia, Phys. Rev. Lett. **108**, 265001 (2012).

[61] B. Labit, I. Furno, A. Fasoli, A. Diallo, S. H. Müller, G. Plyushchev, M. Podestà, and F. M. Poli, Phys. Rev. Lett. **98**, 255002 (2007).

[62] F. Sattin, M. Agostini, P. Scarin, N. Vianello, R. Cavazzana, L. Marrelli, G. Serianni, S. J. Zweben, R. J. Maqueda, Y. Yagi, H. Sakakita, H. Koguchi, S. Kiyama, Y. Hirano, and J. L. Terry, Plasma Phys. Control. Fusion **51**, 055013 (2009).

[63] F. Sattin, M. Agostini, R. Cavazzana, G. Serianni, P. Scarin, and N. Vianello, Phys. Scr. **79**, 045006 (2009).

[64] M. A. Pedrosa, C. Hidalgo, B. A. Carreras, R. Balbín, I. García-Cortés, D. Newman, B. van Milligen, E. Sánchez, J. Bleuel, M. Endler, S. Davies, and G. F. Matthews, Phys. Rev. Lett. **82**, 3621 (1999).

[65] B. A. Carreras, R. Balbín, B. van Milligen, M. A. Pedrosa, I. Garcia-Cortes, E. Sanchez, C. Hidalgo, J. Bleuel, M. Endler, H. Thomsen, A. Chankin, S. Davies, K. Erents, and G. F. Matthews, Phys. Plasmas **6**, 4615 (1999).

[66] O. E. Garcia, R. Kube, A. Theodorsen, B. LaBombard, and J. L. Terry, Phys. Plasmas **25**, 056103 (2018).

[67] J. A. Boedo, D. L. Rudakov, R. Moyer, S. I. Krasheninnikov, D. Whyte, G. McKee, G. Tynan, M. Schaffer, P. C. Stangeby, P. West, S. L. Allen, T. Evans, R. Fonck, E. Hollmann, A. Leonard, A. Mahdavi, G. Porter, M. Tillack, and G. Y. Antar, Phys. Plasmas **8**, 4826 (2001).

[68] D. L. Rudakov, J. A. Boedo, R. A. Moyer, S. I. Krasheninnikov, A. W. Leonard, M. A. Mahdavi, G. R. McKee, G. D. Porter, P. C. Stangeby, J. G. Watkins, W. P. West, D. G. Whyte, and G. Y. Antar, Plasma Phys. Control. Fusion **44**, 308 (2002).

[69] O. E. Garcia, S. M. Fritzner, R. Kube, I. Cziegler, B. LaBombard, and J. L. Terry, Phys. Plasmas **20**, 055901 (2013).

[70] O. E. Garcia, I. Cziegler, R. Kube, B. LaBombard, and J. L. Terry, J. Nucl. Mater. **438**, S180 (2013).

[71] O. E. Garcia, J. Horacek, and R. A. Pitts, Nucl. Fusion **55**, 062002 (2015).

[72] G. Y. Antar, G. Counsell, and J. W. Ahn, Phys. Plasmas **12**, 1 (2005).

[73] Y. Marandet, N. Nace, M. Valentinuzzi, P. Tamain, H. Bufferand, G. Ciraolo, P. Genesio, and N. Mellet, Plasma Phys. Control. Fusion **58**, 114001 (2016).

[74] S. O. Rice, Bell Syst. Tech. J. **23**, 282 (1944).

[75] S. O. Rice, Bell Syst. Tech. J. **24**, 46 (1945).

[76] J. R. Myra and D. A. D'Ippolito, Phys. Plasmas **17**, 102510 (2010).

[77] A. K. Ram, K. Hizanidis, and Y. Kominis, Phys. Plasmas **20**, 056110 (2013).

[78] B. LaBombard, E. Marmar, J. Irby, J. L. Terry, R. Vieira, G. Wallace, D. G. Whyte, S. Wolfe, S. Wukitch, S. G. Baek, W. Beck, P. Bonoli, D. Brunner, J. Doody, R. Ellis, D. Ernst, C. Fiore, J. P. Freidberg, T. Golfinopoulos, R. Granetz, M. Greenwald, Z. S. Hartwig, A. Hubbard, J. W. Hughes, I. H. Hutchinson, C. Kessel, M. Kotschenreuther, R. Leccacorvi, Y. Lin, B. Lipschultz, S. Mahajan, J. Minervini, R. Mumgaard, R. Nygren, R. Parker, F. Poli, M. Porkolab, M. L. Reinke, J. Rice, T. Rognlien, W. Rowan, S. Shiraiwa, D. Terry, C. Theiler, P. Titus, M. Umansky, P. Valanju, J. Walk, A. White, J. R. Wilson, G. Wright, and S. J. Zweben, Nucl. Fusion **55**, 053020 (2015).

[79] N. Campbell, Proc. Camb. Philol. Soc. **15**, 117 (1909).

[80] J. R. Segal, B. Ceccarelli, R. Fesce, and W. P. Hurlbut, Biophys. J. **47**, 183 (1985).

[81] R. Fesce, J. Gen. Physiol. **88**, 25 (1986).

[82] J.-W. Jang, J. Risk Insur. **71**, 201 (2004).

[83] P. Claps, A. Giordano, and F. Laio, Adv. Water Resour. **28**, 992 (2005).

[84] M. Lefebvre, Stat. Probab. Lett. **78**, 3274 (2008).

[85] E. Daly and A. Porporato, Phys. Rev. E **81**, 061133 (2010).

[86] Z. Elter, C. Jammes, I. Pázsit, L. Pál, and P. Filliatre, Nucl. Instruments Methods Phys. Res. Sect. A Accel. Spectrometers, Detect. Assoc. Equip. **774**, 60 (2015).

[87] A. Theodorsen, O. E. Garcia, R. Kube, B. LaBombard, and J. L. Terry, "Universality of Poisson-driven plasma fluctuations in the Alcator C-Mod scrape-off layer," ready for submission, arXiv:1802.05052 .

[88] O. E. Garcia, R. Kube, A. Theodorsen, and H. L. Pécseli, Phys. Plasmas **23**, 052308 (2016).

[89] E. Parzen, *Stochastic Processes* (Society for Industrial and Applied Mathematics, Philadelphia, 1999).

[90] L. Bondesson, Adv. Appl. Probab. **14**, 855 (1982).

[91] O. E. Garcia and A. Theodorsen, Phys. Plasmas **24**, 020704 (2017).

[92] O. E. Garcia and A. Theodorsen, Phys. Plasmas **24**, 032309 (2017).

[93] H. Biermé and A. Desolneux, J. Appl. Probab. **49**, 100 (2012).

[94] J. E. Maggs and G. J. Morales, Phys. Rev. Lett. **107**, 1 (2011).

[95] B. P. Van Milligen, R. Sánchez, and C. Hidalgo, Phys. Rev. Lett. **109**, 12 (2012).

[96] J. E. Maggs, T. L. Rhodes, and G. J. Morales, Plasma Phys. Control. Fusion **57**, 045004 (2015).

[97] Z. Zhu, A. E. White, T. A. Carter, S. G. Baek, and J. L. Terry, Phys. Plasmas **24**, 042301 (2017).

[98] O. E. Garcia and A. Theodorsen, Phys. Plasmas **25**, 014503 (2018).

[99] O. E. Garcia and A. Theodorsen, Phys. Plasmas **25**, 014506 (2018).

[100] G. Decristoforo, O. E. Garcia, R. Kube, and A. Theodorsen, "Intermittent fluctuations and Lorentzian pulses in flux-driven thermal convection," in preparation.

[101] F. Militello and J. T. Omotani, Nucl. Fusion **56**, 104004 (2016).

[102] F. Militello and J. T. Omotani, Plasma Phys. Control. Fusion **58**, 125004 (2016).

[103] N. R. Walkden, A. Wynn, F. Militello, B. Lipschultz, G. Matthews, C. Guillemaut, J. Harrison, and D. Moulton, Plasma Phys. Control. Fusion **59**, 085009 (2017).

[104] F. Militello, B. Dudson, L. Easy, A. Kirk, and P. Naylor, Plasma Phys. Control. Fusion **59**, 125013 (2017).

[105] A. Theodorsen and O. E. Garcia, Phys. Plasmas **23**, 040702 (2016).

Paper I:
Scrape-off layer turbulence in TCV: evidence in support of stochastic modelling

A. Theodorsen, O. E. Garcia, J. Horacek, R. Kube and R. A. Pitts,
Plasma Physics and Controlled Fusion **58**, 044006 (2016),
doi:10.1088/0741-3335/58/4/044006.

Paper II: Statistical properties of a filtered Poisson process with additive random noise: distributions, correlations and moment estimation

A. Theodorsen, O. E. Garica and M. Rypdal,
Physica Scripta **92**, 054002 (2017),
doi:10.1088/1402-4896/aa694c

Paper III:
Relationship between frequency power spectra and intermittent, large-amplitude bursts in the Alcator C-Mod scrape-off layer

A. Theodorsen, O. E. Garica, R. Kube, B. LaBombard and J. L. Terry,
Nuclear Fusion **57**, 114004 (2017),
doi:10.1088/1741-4326/aa7e4c

Paper IV:
Level crossings and excess times due to a superposition of uncorrelated exponential pulses

A. Theodorsen and O. E. Garcia,
Physical Review E **97**, 012110 (2018),
doi:10.1103/PhysRevE.97.012110

Paper V:
Probability distribution functions for intermittent scrape-off layer plasma fluctuations

A. Theodorsen and O. E. Garcia,
Plasma Physics and Controlled Fusion **60**, 034006 (2018),
doi:10.1088/1361-6587/aa9f9c